Assembly of Mitochondrial Complex I Requires the Low-Complexity Protein AMC1 in *Chlamydomonas reinhardtii*

Nitya Subrahmanian,*,† Andrew David Castonguay,*,‡ Claire Remacle,§ and Patrice Paul Hamel*,,1**

*Department of Molecular Genetics and **Department of Biological Chemistry Pharmacology, The Ohio State University, Columbus, Ohio 43210, †Plant Cellular and Molecular Biology Graduate Program, The Ohio State University, 43210, ‡Molecular Genetics Graduate Program, The Ohio State University, 43210, and §Genetics and Physiology of Microalgae, UR InBios/Phytosystems, University of Liège, 4000, Belgium

ABSTRACT Complex I is the first enzyme involved in the mitochondrial electron transport chain. With >40 subunits of dual genetic origin, the biogenesis of complex I is highly intricate and poorly understood. We used *Chlamydomonas reinhardtii* as a model system to reveal factors involved in complex I biogenesis. Two insertional mutants, displaying a complex I assembly defect characterized by the accumulation of a 700 kDa subcomplex, were analyzed. Genetic analyses showed these mutations were allelic and mapped to the gene *AMC1* (*Cre16.g688900*) encoding a low-complexity protein of unknown function. The complex I assembly and activity in the mutant was restored by complementation with the wild-type gene, confirming AMC1 is required for complex I biogenesis. The N terminus of AMC1 targets a reporter protein to yeast mitochondria, implying that AMC1 resides and functions in the *Chlamydomonas* mitochondria. Accordingly, in both mutants, loss of AMC1 function results in decreased abundance of the mitochondrial *nd4* transcript, which encodes the ND4 membrane subunit of complex I. Loss of ND4 in a mitochondrial *nd4* mutant is characterized by a membrane arm assembly defect, similar to that exhibited by loss of AMC1. These results suggest AMC1 is required for the production of mitochondrially-encoded complex I subunits, specifically ND4. We discuss the possible modes of action of AMC1 in mitochondrial gene expression and complex I biogenesis.

KEYWORDS Energy-transducing membranes; respiration; mitochondrial complex I assembly; *Chlamydomonas reinhardtii*; low-complexity protein; mitochondrial gene expression

THE mitochondria are important organelles for cellular energy production. Mitochondrial ATP synthesis is chemiosmotically coupled to the electron transfer chain (ETC), which is located in the mitochondrial inner membrane (Mitchell 1966). The ETC involves four major membrane-bound complexes that mediate electron transfer from the substrates, NADH, or succinate, to the terminal electron acceptor O_2 (Green and Tzagoloff 1966). Mitochondrial complex I (EC 1.6.5.3) is the first and largest enzyme of the ETC. This multimeric enzyme consists of one flavin mononucleotide molecule and eight iron-sulfur (Fe-S) clusters that catalyze electron transfer from NADH to ubiquinone (Zickermann *et al.* 2009; Letts and Sazanov 2015). Conserved from bacteria to humans, complex I is a major entry point for electrons into the respiratory chain. For each molecule of NADH oxidized by complex I, four protons are pumped from the matrix to the intermembrane space, leading to the production of 2.7 ATP molecules per oxygen atom reduced (Hinkle 2005; Watt *et al.* 2010).

Electron micrography and X-ray crystallography of complex I from multiple organisms have revealed a L-shaped structure, with a hydrophobic arm embedded in the inner mitochondrial membrane and a hydrophilic arm protruding into the matrix (Figure 4B and Figure 6B) (Dudkina *et al.* 2005; Peters *et al.* 2008; Baradaran *et al.* 2013; Vinothkumar *et al.* 2014; Letts and Sazanov 2015; Zickermann *et al.* 2015). The hydrophilic arm contains domains for NADH and ubiquinone binding, whereas the hydrophobic arm is required for proton pumping.

doi: https://doi.org/10.1534/genetics.120.303029
Manuscript received November 11, 2019; accepted for publication February 5, 2020; published Early Online February 19, 2020.
Supplemental material available at figshare: https://doi.org/10.25386/genetics.11872362.
[1]Corresponding author: Department of Molecular Genetics and Department of Biological Chemistry and Pharmacology, 500D Aronoff Laboratory, The Ohio State University, 318 W. 12th Ave., Columbus, OH 43210. E-mail: hamel.16@osu.edu

Eukaryotic complex I consists of >40 nuclear- and mitochondria-encoded subunits (Remacle *et al.* 2008; Subrahmanian *et al.* 2016). Among these, 14 are considered "core" subunits as they are conserved in bacterial complex I and define the minimal requirement for catalytic activity. In addition, 30 or more "accessory" subunits are present, contributing to a total size of ~1 MDa (Remacle *et al.* 2008; Subrahmanian *et al.* 2016). Because of the large number of subunits of dual genetic origin, complex I assembly requires precise coordination of various cellular processes: the transcription of genes encoding subunits, translation of the transcripts in the cytosol and the mitochondria, mitochondrial import of cytosol-synthesized subunits, synthesis and insertion of the cofactors, and the correct folding of each subunit. Subsequently, the hydrophilic and hydrophobic subunits need to be assembled in a step-wise manner into individual modules, which are then combined to form the holoenzyme. This basic model of complex I biogenesis is common for all eukaryotes although the sequence of subunit addition in individual modules may vary according to the organism (Vogel *et al.* 2007). This elaborate process requires the assistance of nonstructural proteins that facilitate each step of biogenesis. Such proteins, referred to as biogenesis/assembly factors, are involved in the various stages of complex I biogenesis, but do not form part of the final holoenzyme (Subrahmanian *et al.* 2016; Guerrero-Castillo *et al.* 2017).

To date, 20 proteins have been associated with mammalian complex I biogenesis, of which 12 have been linked to human diseases (Fassone *et al.* 2010; Sánchez-Caballero *et al.* 2016; Formosa *et al.* 2018). Orthologs for most of the mammalian assembly factors are present in plants, although their function in plant complex I assembly is yet to be experimentally confirmed (Subrahmanian *et al.* 2016). In *Arabidopsis*, a role in complex I assembly has been validated for only three factors: INDH, GLDH [reviewed in Subrahmanian *et al.* (2016)], and CIAF1 (Ivanova *et al.* 2019). INDH, an ortholog of the mammalian factor Ind1, was originally postulated as involved in Fe-S delivery to complex I subunits. However, in *Arabidopsis*, an alternate role in the translation of mitochondrially encoded complex I subunits was demonstrated for INDH (Sheftel *et al.* 2009; Wydro *et al.* 2013). GLDH is a plant-specific assembly factor that localizes in the inner mitochondrial membrane and faces the intermembrane space. *Arabidopsis* GLDH is associated to three sequential, membrane-bound assembly intermediates (Schertl *et al.* 2012; Schimmeyer *et al.* 2016). Finally, CIAF1 is a LYR domain containing mitochondrial matrix protein that interacts with the matrix arm 23 kDa TYKY subunit of complex I (Ivanova *et al.* 2019). Loss of CIAF1 in *Arabidopsis* resulted in the accumulation of the 650 and 800 kDa assembly intermediates. A possible role in Fe-S cluster assembly was postulated based on the ability of CIAF1 to rescue a yeast mutant deficient for Fe-S cluster biogenesis.

Considering the high degree of intricacy in complex I biogenesis, it is reasonable to expect numerous factors remain to be discovered. Very little is known about factors specifically dedicated to the expression of mitochondrially-encoded complex I subunits, except in vascular plants (Braun *et al.* 2014). To identify additional complex I biogenesis factors, we selected the unicellular photosynthetic alga, *Chlamydomonas reinhardtii*, as an experimental system (Remacle *et al.* 2008). The photosynthetic capacity of *Chlamydomonas* allows respiratory mutants to be viable (Cardol *et al.* 2003). This is in contrast to mammalian organisms which cannot survive when respiration is abolished. Additionally, the *Chlamydomonas* ETC contains type-II NADH dehydrogenases, absent in mammalian systems, which can partially compensate for loss of complex I activity (Lecler *et al.* 2012) and allow the survival of complex I-null mutants under respiratory conditions. However, the alternate enzymes cannot contribute to the proton gradient, purportedly decreasing the efficiency of ATP synthesis. Hence, complex I-null mutants exhibit a respiratory growth defect that manifests as a Slow growth In the Dark (SID) phenotype (Remacle *et al.* 2001a; Cardol *et al.* 2002, 2008; Barbieri *et al.* 2011). Utilizing this SID phenotype, a number of mutants for mitochondria- and nuclear-encoded complex I subunits have been isolated in *Chlamydomonas* [reviewed in Salinas *et al.* (2014)], providing valuable insights into the sequence of complex I assembly in this organism. So far, only one biogenesis factor, the NDUFAF3 ortholog, has been experimentally confirmed as required for *Chlamydomonas* complex I assembly (Massoz *et al.* 2017).

In this study, we report a previously unidentified biogenesis factor, AMC1, required for the assembly of the distal membrane arm of complex I. We show that the N terminus of AMC1 is capable of targeting a reporter protein to the mitochondria. Loss of AMC1 specifically affects the abundance of mitochondrial *nd4* transcript, implicating a role for AMC1 in mitochondrial gene expression, a poorly understood process in *Chlamydomonas*.

Materials and Methods

Strains and culture conditions

Chlamydomonas strains were grown in liquid or solid medium: Tris-acetate-phosphate (TAP), with 20 mM Tris-base and 17 mM acetic acid, or Tris-acetate-phosphate supplemented with arginine (1.9 mM) (TARG) (Harris 1989). For some strains, TARG supplemented with 25 μg/ml hygromycin B, or TARG supplemented with 25 μg/ml paromomycin, was used. Algal strains were grown at 25°, in continuous light at 50 μmol/m^2/sec or in the dark.

Wild-type strains 3A$^+$ (*mt*$^+$; *arg7-8*) and 4C$^-$ (*mt*$^-$; *arg7-8*), derived from genetic crosses of the CC124 background strain, were used for generating the insertional mutants (provided by Dr. Rochaix, University of Geneva, Switzerland). The insertional mutagenesis was conducted as described in Barbieri *et al.* (2011). The original complex I mutants *amc1 (4C10)* strain (*mt*$^+$; *amc1-1*; *APHVII*; *arg7-8*), *amc5 (87D3)* strain (*mt*$^+$; *nuob10*::*APHVIII*; *arg7-8*) (Barbieri *et al.* 2011), *amc11 (10G11)* strain (*mt*$^-$; *amc1-2*; *APHVII*; *arg7-8*) (Subrahmanian *et al.* 2020), and their derivatives were used. In addition, the following haploid progeny obtained via genetic crosses were also used: *amc11 (65)* (*mt*$^-$; *amc1-2*;

APHVII) derived from *10G11*, *amc1(2) (mt*$^+$; *amc1-1)*, and *amc1(27) (mt*$^-$; *amc1-1*; *arg7-8)* derived from *4C10*. The *amc5* strain complemented with the wild-type *NUOB10* gene is referred to as [*amc5*; *NUOB10*]. The Δ*nd4* strain was generated from the *dum11* strain (Dorthu *et al.* 1992). Generation of strains from genetic crosses is detailed in Supplemental Material, Method S1. The key strains used in this study and their corresponding reference numbers in the *Chlamydomonas* Resource Center are listed in Table S1.

Saccharomyces cerevisiae strain JM45 Δ*coq3* (*MAT*α, *his4-580*, *leu2-3,112*, *trp1-289*, *ura3-52*, *coq3*::*LEU2)* (Clarke *et al.* 1991) was grown at 28° in liquid or solid medium, containing glucose as the fermentable substrate or ethanol as the respiratory substrate (Dujardin *et al.* 1980). Strains were transformed by the one-step transformation method (Chen *et al.* 1992; Saint-Georges *et al.* 2002).

Chemo-competent *Escherichia coli* DH5α strains were used for molecular cloning. *E. coli* was grown at 37° in Luria-Bertani broth and Luria-Bertani agar according to Silhavy *et al.* (1984).

Ten-fold dilution series

One loop of cells grown for 3–5 days on solid TARG plates were resuspended in 500 μl of liquid TARG medium. The cell density was measured spectrophotometrically at OD_{750} and diluted to an OD_{750} = 2.0. This normalized suspension was used as the starting material (1) for making five serial 10-fold dilutions (10^{-1}, 10^{-2}, 10^{-3}, 10^{-4}, and 10^{-5}). A volume of 8 μl for each dilution was plated on solid TARG plates. For scoring the SID phenotype, two plates were prepared simultaneously and incubated at 25°, one in continuous light and another in the dark, for at least 7 days. Ten-fold dilution series on yeast strains were conducted as described above, except that cells collected from solid medium were resuspended in sterile water. The cell density for yeast strains was measured spectrophotometrically at A_{600} and normalized to an OD_{600} = 1.0. The cells were plated on two solid media and incubated at 28°: single dropout synthetic medium lacking uracil (fermentable medium), and rich ethanol-containing medium (respiratory medium).

Growth curves

Liquid cultures were inoculated with a starting cell density of 10^5 cells/ml in 50 ml TARG cultures. For each strain, three biological replicates were inoculated in continuous light at 25 μmol/m^2/sec and in the dark. Cell density was evaluated every 8 hr by measuring optical density at A_{750} (Lapaille *et al.* 2010), over a period of 10 days. Growth rate μ was calculated as $3.3 \times (\log_{10}N - \log_{10}N_0)/(t_N - t_0)$, where N is the final cell density at time t_N and N_0 is the initial cell count at time t_0. The generation time was calculated as $1/\mu$ (Harris 1989; Kropat *et al.* 2011). The generation time for the strains in the light were determined between 36 and 108 hr, except for *amc1-2* (48–120 hr). The generation times for the strains in the dark were calculated between 36 and 156 hr, except for *amc1-2*, which was calculated between 72 and 240 hr. The wild-type and the *amc1-2* strain used were 4C$^-$ and *amc11 (10G11)*, respectively.

Enzymatic activity assays

Mitochondrial enzymatic activity measurements were conducted as described previously in Remacle *et al.* (2001b) and (2004), and Cardol *et al.* (2002), with slight modifications. Cells grown for 2–3 days on solid medium were resuspended in MOPS-KOH extraction buffer (10 mM MOPS-KOH, pH 7.4, 0.5 M mannitol, 100 mg/ml BSA, 0.5 mM PMSF). Cells were lysed by sonication using a Branson Sonifier 150 (1/8 inch probe tip), at 12 W output for 2 × 30 sec. Following lysis, the extract was centrifuged at 480 × *g* for 10 min, followed by 3000 × *g* for 5 min; the supernatant was centrifuged at 27,000 × *g* for 20 min, and the resulting pellet was the crude membrane extract. Complex I activity was determined as the rate of NADH oxidation, which was measured spectrophotometrically at A_{340}. The substrates used were 100 μM NADH (0384-1G; Amresco) and 100 μM duroquinone (D22320-4; Sigma-Aldrich). Specific activity was calculated using the molar extinction coefficient for NADH at $\varepsilon_{340\ nm}$ = 6.22 mM^{-1} cm^{-1} in the absence and presence of 45 μM rotenone (150154; MP Biomedicals), a complex-I-specific inhibitor. Complex II + III activity was determined as the rate of cytochrome *c* reduction and measured spectrophotometrically at A_{550}. It was conducted in the presence of 20.25 mM succinate (158751000; Acros Organics), 1 mM KCN (P223I-100; Fisher Scientific), and 56 μM equine heart cytochrome *c* (2506–500 mg; Sigma, St. Louis, MO). Complex II + III activity was calculated using molar extinction coefficient for cytochrome *c* at $\Delta\varepsilon_{550nm}$ = 19.6 mM^{-1} cm^{-1}, in the absence and presence of complex-III-specific inhibitor myxothiazol (3 μM) (T5580; Sigma). Complex IV activity assay was conducted in the presence of 1% Triton X-100 and 56 μM reduced cytochrome *c*. Cytochrome *c* was reduced with two times the amount of sodium dithionite and purified with a PD10-desalting column with sephadex G-25 resin (17085101; GE Healthcare Life Sciences) according to the manufacturer's protocol. Complex IV activity was calculated using molar extinction coefficient for cytochrome *c* at $\Delta\varepsilon_{550\ nm}$ = 19.6 mM^{-1} cm^{-1}, in the absence and presence of KCN (1 mM).

Blue-native polyacrylamide gel electrophoresis and in-gel activity

Partially purified membranes were extracted as described for enzymatic activity measurement. Complexes were separated by blue-native polyacrylamide gel electrophoresis (BN-PAGE) using 4–12% (w/v) acrylamide gradient gels as described in Schägger and von Jagow (1991). Membranes were partially solubilized as described below. Membrane proteins (500 μg) were pelleted at 18,000 × *g* for 20 min at 4°. The membranes were then resuspended in 180 μl of 2% (w/v) sodium *n*-dodecyl-β-D maltoside (40430017-3; Bioworld) and incubated on wet ice for 1 hr. Unsolubilized membrane particles were removed by centrifugation at 18,000 × *g* for 20 min at 4°. To the supernatant, 20 μl of

10% (w/v) sodium taurodeoxycholate hydrate (T-0875; Sigma) was added (Cardol *et al.* 2006). Both *n*-dodecyl-β-D maltoside and taurodeoxycholate hydrate were dissolved in ACA buffer (750 mM aminocaproic acid, 0.5 mM EDTA, 50 mM Bis-Tris, pH 7.0). Partially solubilized membrane protein (200 μg) were loaded per lane. *In-gel* NADH dehydrogenase (complex I) activity was visualized as purple bands after incubating the gels in 100 mM MOPS buffer, pH 8, containing 1 mg/ml *p*-nitro blue tetrazolium chloride (NBT; NBT2.5; Goldbio) and 0.2 mM NADH.

Immunoblotting analysis

For SDS-PAGE, 10 μg of proteins were separated by 12.5% acrylamide gel and immunoblotting was performed according to established protocols (Sambrook *et al.* 1989). For BN-PAGE, protein complexes were prepared and separated as described previously. Custom-made primary antibodies raised against *Chlamydomonas* complex I subunits 51 and 49 kDa, and TYKY subunits (referred to as NUO6, NUO7, and NUO8 in *Chlamydomonas*, respectively) were used [from Genescript, as described in Barbieri *et al.* (2011)]. Protein complexes separated via BN-PAGE were immunodecorated with 1:3000 diluted α-51 kDa or 1: 3000 diluted α-49 kDa overnight at 4°. Protein extracts resolved via SDS-PAGE were immunodetected with 1:3000 diluted α-51 kDa, 1: 3000 diluted α-49 kDa, 1:2000 diluted α-TYKY, and 1:12,000 diluted α-cyt *f* for 3 hr at room temperature. The secondary antibody used was 1:10,000 diluted HRP-conjugated anti-rabbit goat antibody (170-6515; Bio-Rad, Hercules, CA) and incubated at room temperature for 2 hr.

Additional procedures

The Supplemental Material details procedures for molecular methods such as diagnostic PCRs, thermal asymmetric thermal assymetric interlaced PCRs (TAIL-PCRs), PCR-based cosmid screening, biolistic transformation, quantitative RT-PCRs, and plasmid construction in Methods S2–S7, respectively. Primer sequences are provided in Tables S2 and S3.

Data availability

Strains and plasmids are available upon request. The authors affirm that all data necessary for confirming the conclusions of the article are present within the article, figures, tables, and supplemental information. Supplemental material available at figshare: https://doi.org/10.25386/genetics.11872362.

Results

Two complex I mutants harbor mutations in the same gene AMC1

A forward genetic screen was executed to isolate complex I mutants in *Chlamydomonas* (Barbieri *et al.* 2011; Subrahmanian *et al.* 2020). Insertional mutagenesis was conducted using the wild-type strain as a recipient with the iHyg3 cassette which encodes the *APHVII* transgene and confers hygromycin B resistance. In this study, we investigated two insertional *amc* (**a**ssembly of **m**itochondria**l** **c**omplex I) mutants, *amc1* (Barbieri *et al.* 2011) and *amc11* (Subrahmanian *et al.* 2020), that display a characteristic SID phenotype with severe complex I deficiency (Figure 1, A and B).

Previous analyses of *amc1* had shown the SID phenotype did not cosegregate with the insertional cassette (Barbieri *et al.* 2011) and the *AMC1* locus had remained unidentified. Since the *amc11* mutant was also generated by insertional mutagenesis, we first tested if the complex I deficiency was linked to the insertional cassette via genetic analyses. Segregation of the SID phenotype and hygromycin B resistance (HyB^R) was monitored in the meiotic progeny obtained from the cross of *amc11* × wild type (Table 1). All the HyB^R meiotic progeny (total, 59) displayed a SID phenotype, while the hygromycin B sensitive (HyB^S) progeny (total, 96) displayed wild-type growth in the dark. Cosegregation of the SID phenotype with HyB^R indicates that the *amc11* mutation is tightly linked to the insertional cassette.

To test if the *amc11* mutation is allelic to the previously isolated *amc* mutants (Barbieri *et al.* 2011), vegetative diploids were generated. Upon testing the respiratory growth phenotype, *amc11/amc1* diploids revealed a SID phenotype (Figure 1A). In addition, a total of 98 meiotic progeny obtained from an *amc1* × *amc11* cross displayed a SID phenotype. From these genetic analyses, we concluded that the mutations in *amc11* and *amc1* define the same genetic locus.

To map the mutations in the *amc11* and *amc1* strains, we conducted molecular analyses. The linkage between the insertional cassette and complex I deficiency in the *amc11* mutant can be attributed to the inactivation of a gene involved in complex I function by the insertional marker. Hence, we sought to retrieve the genomic sequence flanking the insertional cassette via TAIL-PCR. The mutation was mapped to exon 2 of the gene *Cre16.g688900* of unknown function (Figure 1C and Figure S1). A truncated form of the iHyg3 cassette, lacking the first 123 bp of the *TUB2* promoter, was inserted at this site. The insertional event was accompanied by a deletion of 42 bp of the genomic DNA at the site of insertion in the *Cre16.g688900* gene. Concomitant with the cassette insertion was the cointegration of foreign DNA (568 and 42 bp at the 5′- and 3′- ends of the cassette, respectively) corresponding to the herring sperm DNA used as a carrier during transformation (Shimogawara *et al.* 1998). Although herring sperm DNA sequence is currently unavailable, similarity searches using NCBI BLAST indicated the sequence integrated at the 5′-end displays 94% identity to arctic cod fish DNA (*Boreogadus saida*).

In accordance with the TAIL-PCR analyses, DNA amplification of a region spanning the site of insertion in exon 2 (Figure 1D, amplicons B and C) failed to amplify in the *amc11* mutant, but was amplified in the wild type, confirming an insertion is present at this site. In addition, DNA was amplified, specifically in the *amc11* mutant and not in the wild type, at the 3′-end junction between the cassette and the genomic region (Figure 1D, amplicon E). Therefore, the *amc11* mutation is caused by a 2.23 kb insertional sequence,

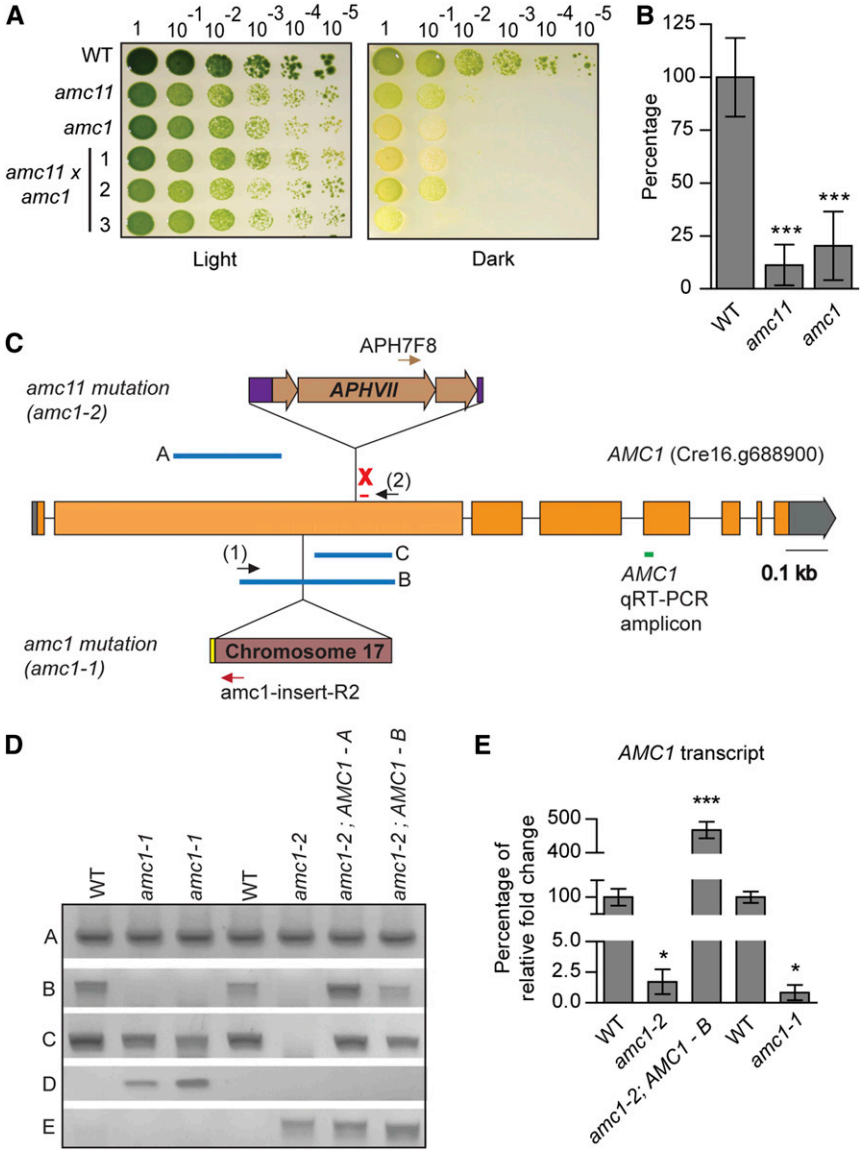

Figure 1 The insertional mutations in the *amc1* and *amc11* mutants are allelic. (A) The SID phenotype of the *amc1* and *amc11* mutants with three independent *amc1* × *amc11* diploids was tested by 10-fold dilution series. The dilutions were plated on acetate-containing medium and incubated, in the light and in the dark, for 16 days. (B) Complex I (rotenone-sensitive NADH: duroquinone oxidoreductase) activity was determined for the haploid strains shown in A from six biological replicates. The average complex I activity of WT ($4C^-$) is 67.7 ± 12.61 nmol NADH oxidized/min/mg protein. The activities are represented as percentage of WT. The significance of complex I deficiency with respect to WT was determined by two-tailed unequal variances *t*-test and the symbol *** $P < 0.001$. (C) The positions of the insertional mutations in the *Cre16.g688900 (AMC1)* gene of the *amc1* and the *amc11* mutants are represented here. The gray rectangles indicate UTRs, the orange rectangles indicate the regions of the exons corresponding to the coding sequence, and the black lines correspond to the introns of the *AMC1* gene, as predicted by the *Chlamydomonas* genome database v5.5. In the *amc11* mutant, the insertional mutation is caused by the iHyg3 cassette. The red symbol "X" marks the location of the 42 bp deletion in *AMC1* of the *amc11* mutant. The purple rectangles in the inserted sequence represent the 568 and 42 bp sequences that cointegrated at the 5′- and 3′-ends of the cassette, respectively. In the *amc1* mutant, the insertional mutation is a 1.535 kb sequence of an intergenic region from chromosome 17. The yellow rectangle represents 28 bp of random DNA cointegrated at the 5′-end of the insertion site. The blue lines indicate the genomic DNA regions (A–C) amplified by PCR (Figure 1D). The brown, red, and black arrows represent the primers specific for the iHyg3 cassette, chromosome 17 intergenic DNA, and *AMC1*, respectively, used to amplify amplicons D and E in panel D. The green line indicates the region of transcript amplified for quantitative RT-PCR in panel E. (D) The molecular lesions in *AMC1* were confirmed by diagnostic PCR using *AMC1*-specific primers. Two *amc1-1* strains, the original *amc1* (*4C10*) and a haploid progeny *amc1* (*27*), and the *amc1-2* strain *amc11* (*10G11*) were used to confirm the mutation in *AMC1*. Amplicons D and E were amplified with primers indicated in panel C: D [10G11 exon2F (1)/amc1-insert-R2]; E [APH7F8/10G11 AD1-F (2)]. (E) Real-time quantitative PCR was used to assess the quantity of *AMC1* messenger RNA relative to three reference transcripts *TUA2*, *EIFA*, and *CBLP*. The average was obtained from three biological replicates, each including two technical replicates. The error bars represent SD of the mean. The results are represented as percentage of fold change relative to respective WT ($3A^+$ for *amc1-1* and $4C^-$ for *amc1-2* and [*amc1-2*; *AMC1-B*]). The *amc1-1* and *amc1-2* strains tested here are *amc1 (4C10)* and *amc11 (10G11)*, respectively. Statistical significance was determined by two-tailed unequal variances *t*-test. * $P < 0.05$, *** $P < 0.001$. WT, wild type.

consisting of iHyg3 cassette and herring sperm DNA, in exon 2 of *Cre16.g688900*.

Since the *amc1* mutation is allelic to the *amc11* mutation, we expected the *Cre16.g688900* gene to harbor a molecular lesion in the *amc1* strain. To determine if *amc1* is characterized by a mutation in this gene, we performed diagnostic PCRs on two *amc1* strains, across the full length of the *Cre16.g688900* gene. Similar to the *amc11* mutant, a region of exon 2 did not amplify in the *amc1* mutant strains (Figure 1D, amplicon B). The primer-binding sites for amplicon B are present in amplicons A and C, which are successfully amplified in the *amc1* mutant. Since we failed to detect a smaller amplicon B, we can rule out the occurrence of a major deletion. Therefore, the failure to detect amplicon B is suggestive of an insertion present in exon 2 of the *Cre16.g688900* gene in the *amc1* mutant. In addition, a region spanning the *amc11* insertion site amplified in the *amc1* mutant strains but failed to amplify in the *amc11* mutant, indicating that the insertion in *amc1* is upstream of the insertional site in *amc11* (Figure 1D, amplicon C). Since the insertional cassette is not linked with the *amc1* mutation, we hypothesized that the insertion in *amc1* is caused either by a truncated and nonfunctional cassette, the herring sperm DNA used for mutagenesis, or fragments of *Chlamydomonas* genomic DNA.

Table 1 The *amc11* mutation is linked to the insertional cassette

Parent strain mt^+		Parent strain mt^-		Meiotic progeny		
Strain	Phenotype	Strain	Phenotype	Phenotype	Total	SID
WT	arg^+, HyB^S	*amc11*	arg^-, HyB^R	arg^+, HyB^S	65	0
				arg^-, HyB^S	31	0
				arg^-, HyB^R	34	34
				arg^+, HyB^R	25	25
					155	59

Meiotic progeny from the *amc11* × WT cross were plated on TARG medium and haploid progeny of all phenotypes were obtained by bulk germination. The relevant phenotypes were tested by replica-plating. WT and *amc11* strains used here are 1′ strain and *10G11*, respectively. WT, wild type; arg^+, arginine prototrophic strain; arg^-, arginine auxotrophic strain; HyB^R, hygromycin B resistance; HyB^S, hygromycin B sensitivity.

Insertional mutations caused by *Chlamydomonas* genomic DNA have been previously observed and are proposed to be caused by the integration of extracellular genomic DNA from lysed cells and uptaken during the transformation procedure (Zhang *et al.* 2014). To retrieve the insertional sequence in the *amc1* mutant, TAIL-PCR was performed with *Cre16.g688900*-specific primers. We discovered that the *amc1* mutation was caused by the insertion of a 1.535 kb section of *Chlamydomonas* genomic DNA, identical to an intergenic region from chromosome 17, in the reverse orientation (Figure 1C and Figure S2). The insertion in *amc1* was accompanied by a 28 and a 10 bp insertion of random DNA at the 5′- and 3′-ends of the insertion site, respectively. The 28 bp sequence consists of 18 bp identical to an intron of an unrelated gene, *Cre16.g695800*. As predicted by diagnostic PCRs, the insertional site of the *amc1* mutation is 597 bp upstream of the *amc11* mutation. Further diagnostic PCRs conducted with *Cre16.g688900*-specific and inserted sequence-specific primers (Figure 1D, amplicon D) yielded amplicons of expected size only in the *amc1* mutants, confirming that the intergenic region from chromosome 17 is inserted in exon 2. Additional PCR analyses confirmed that there were no other major rearrangements present in the *Cre16.g688900* gene in the *amc1* or the *amc11* mutant strains. From these results, we conclude that the *amc1* and the *amc11* mutants carry insertional mutations mapping to the *Cre16.g688900* gene. Based on its role in complex I function, this gene shall henceforth be referred to as *AMC1*. In the rest of this manuscript, the allelic mutations in the *AMC1* gene present in the *amc1* and *amc11* strains shall be referred to as *amc1-1* and *amc1-2*, respectively.

To test if the insertional mutations in the *AMC1* coding sequence affected *AMC1* transcript levels, we conducted real-time quantitative RT-PCR analyses (Figure 1E). The *AMC1* transcript levels in the *amc1-1* and *amc1-2* mutants were significantly decreased (Figure 1E). The primers used for quantitative PCR analysis bind downstream of the insertion sites (green line in Figure 1C) and hence, the residual transcript levels detected could be caused by a chimeric transcript produced from the promoter elements present in the cassette or the intergenic region at the insertion site (de Montaigu *et al.* 2010). Since the *amc1-1* and *amc1-2* insertional mutations interrupt the coding sequence at ~3–4 kb from the start codon, we concluded that no full-length transcripts are produced in either mutant.

The AMC1 gene restores complex I activity and assembly in the amc1-2 mutant

The *AMC1* gene does not encode for any known complex I subunits or assembly factors (Subrahmanian *et al.* 2016). To test if the mutation in this gene is responsible for complex I deficiency, we complemented the *amc1-2* strain with the wild-type *AMC1* gene (Figure S3A). For this purpose, we transformed the *amc1-2* mutant with a cosmid (cosmid A) carrying the *AMC1* gene. The transformant, referred to as [*amc1-2*; *AMC1-A*], was restored for complex I activity (Figure 2A). In addition to the *AMC1* gene, cosmid A contains two full-length genes (Figure S3A). To test that the *AMC1* gene is solely responsible for the restoration of complex I proficiency, a truncated form of the cosmid (referred to as cosmid B) containing only the full-length gene *AMC1* was generated (Figure S3A). The *amc1-2* strain transformed with cosmid B, referred to as [*amc1-2*; *AMC1-B*], also showed restoration of complex I activity to wild-type levels, confirming that the disruption in the *AMC1* gene is responsible for the complex I defect (Figure 2A). As expected, complementation with the wild-type *AMC1* gene also resulted in restoration of the *AMC1* transcript levels in the [*amc1-2*; *AMC1-A*] and [*amc1-2*; *AMC1-B*] strains (Figure 1E and Figure S4). In fact, the *AMC1* transcript in [*amc1-2*; *AMC1-B*] showed a fivefold increase compared to the wild type (Figure 1E). Since the introduced *AMC1* gene is under the control of its native promoter, the increase in transcript levels is most likely due to the genomic location of the integrated wild-type gene, which we presume promotes increased *AMC1* expression in this transformant.

To test if the mutation in the *AMC1* gene affects other respiratory complexes, complex II + III and complex IV activities were also determined. The *amc1-2* mutant and the corresponding complemented strains had wild-type levels of complex II + III and complex IV activities (Figure 2, B and C). We concluded that the *amc1-2* mutation, similar to the *amc1-1* mutation (Barbieri *et al.* 2011), only affects complex I.

Alongside the enzymatic analyses, we documented the effect of complementation on the growth phenotype of the *amc1-2* mutant by assessing growth in liquid and solid medium (Figure 3 and Figure S3). In accordance with the previously observed SID phenotype, the *amc1-2* mutant clearly displayed a slower growth rate in the dark, with a generation time of 45 hr, as opposed to the 28 hr for the wild-type strain. The [*amc1-2*; *AMC1-A*] and [*amc1-2*; *AMC1-B*] strains have a generation time of 24 hr in the dark, an indication that growth in respiratory conditions is fully restored (Figure 3A and Figure S3B). A rescue of the growth phenotype in the dark was also observed on solid medium (Figure 3B). Interestingly, the *amc1-2* mutant displayed a longer doubling time in the light (23 hr) compared to wild type (14 hr). This 1.6-fold slower

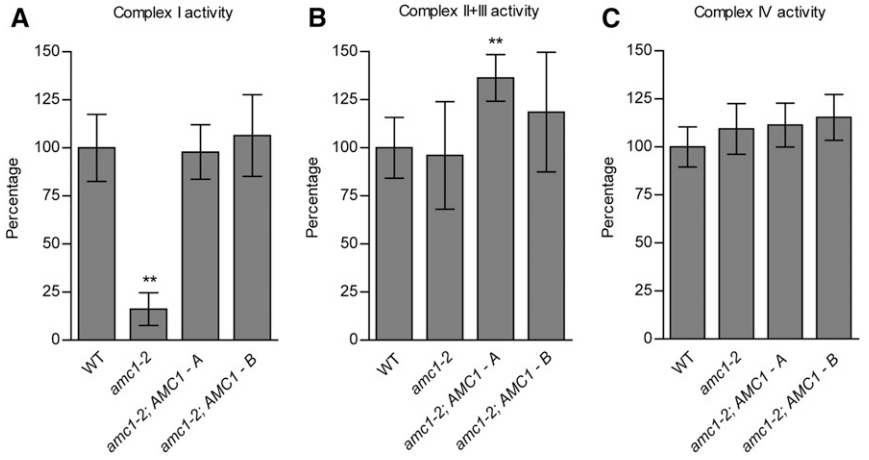

Figure 2 The *AMC1* gene restores complex I proficiency to the *amc1-2* mutant. Enzymatic assays were conducted on partially purified membranes. The activities are displayed as percentage of the mean activity of wild type (WT), with the error bars indicating the percentage of SD relative to the mean. The WT and *amc1-2* strains used are $4C^{-}$ and *amc11 (10G11)*, respectively. The *amc1-2* strain was transformed with cosmids containing the full-length *AMC1* gene. The transformants containing the full cosmid (cosmid A) and the truncated cosmid (cosmid B) are referred to as [*amc1-2*; *AMC1 – A*] and [*amc1-2*; *AMC1 – B*], respectively. (A) Complex I (rotenone-sensitive NADH: duroquinone oxidoreductase) activity was determined from four biological replicates. The average complex I activity of WT is 69.28 ± 12.08 nmol NADH oxidized/min/mg protein. Statistical significance was determined by two-tailed unequal variances *t*-test and the symbol ** ($P < 0.01$). The *amc1-2* mutant has significantly lower complex I activity compared to the WT ($P = 0.00122$). There is no significant difference between the activities measured for the *amc1-2*; *AMC1* and WT strains. However, there is a significant difference between (1) *amc1-2* and [*amc1-2*; *AMC1-A*] ($P = 0.00039$), and (2) *amc1-2* and [*amc1-2*; *AMC1-B*] ($P = 0.002545$). (B) Complex II + III (succinate: cytochrome *c* oxidoreductase) activity was determined from six independent biological replicates. The WT displayed an activity of 30.05 ± 4.76 nmol cytochrome *c* reduced/min/mg protein. The *amc1-2* mutant displayed wild-type levels of complex II + III activity. The [*amc1-2*; *AMC1-A*] strain displays significantly higher activity ($P = 0.002$). (C) Complex IV (cytochrome *c* oxidase) activity was determined from four independent biological replicates. The WT displayed an activity of 248.52 ± 25.8 nmol cytochrome *c* oxidized/min/mg protein.

growth rate in the light for the *amc1-2* mutant correlates with the smaller colonies observed during growth in the light on solid medium (Figure 3B). This phenotype has been previously observed for other complex I mutants as both photosynthesis and respiration contribute to the growth of cells in the light in acetate-containing medium (Remacle *et al.* 2008). The doubling time in the light was restored to wild-type levels upon complementation.

To determine the requirement of AMC1 for complex I assembly, mature complex I and partially assembled subcomplexes were separated by BN-PAGE. *In-gel* NBT staining assessing NADH dehydrogenase activitiy revealed mature complex I as a purple band at ~950 kDa in the wild type (Figure 4). Purple bands seen at higher molecular weights could be due to differential solubilization of membranes or association of complex I with other respiratory complexes such as complexes I + III_2 (Cardol *et al.* 2008). The accumulation of a 700 kDa subcomplex was observed in the *amc1-1* and the *amc1-2* mutants by *in-gel* staining and/or immunoblotting (Figure 4, A and C and Figure S5). However, the 700 kDa subcomplex is highly labile and its detection varies among independent membrane extractions (Barbieri *et al.* 2011). The 700 kDa subcomplex also accumulates in the *nuob10*-null mutant (*amc5*), and the *nd4* and *nd5* mitochondrial mutants, because they lack membrane subunits required for the assembly of the distal membrane arm (Figure 4, A–C) (Cardol *et al.* 2002, 2008; Remacle *et al.* 2006; Barbieri *et al.* 2011). These results suggest that complex I membrane arm assembly was compromised in the *amc1-1* and *amc1-2* mutants. This assembly defect was corrected upon complementation with the wild-type *AMC1* gene (Figure 4). In addition to a subcomplex, lower levels of mature complex (at 950 kDa) can be detected in some extractions in the *amc1-1* mutant by *in-gel* staining and immunoblotting (Figure 4, A and C). Similar to the *amc1-1* mutant, traces of a 950 kDa complex was occasionally observed in the *amc1-2* mutant in certain membrane preparations (Figure S5). From these results, we conclude that AMC1 plays a role in complex I membrane arm assembly.

Previously, it was observed that complex I deficiency results in decreased accumulation of complex I subunits (Saada *et al.* 2009; Barbieri *et al.* 2011; Massoz *et al.* 2017). Indeed, the *amc1-1* mutant displayed decreased steady-state levels of the 51 and 49 kDa, and TYKY subunits (referred to as NUO6, NUO7, and NUO8 in *Chlamydomonas*, respectively) (Barbieri *et al.* 2011). Similar to the *amc1-1* mutant, the *amc1-2* mutant also accumulated lower levels of these three subunits (Subrahmanian *et al.* 2020), the levels of which were restored by complementation with the wild-type *AMC1* gene (Figure 4D). In summary, we have identified *AMC1* as a gene required for complex I assembly and activity.

The N terminus of AMC1 carries a mitochondrial targeting signal

According to the *Chlamydomonas* genome database JGI v5.5, the *AMC1* 8022 bp transcript specifies a large hypothetical protein of 2566 amino acids. No cloned complementary DNAs were available for *AMC1* to corroborate the predicted coding sequence (Asamizu *et al.* 2000). To confirm the predicted coding sequence, RT-PCR was performed on total RNA isolated from the wild-type strain. Amplification of the *AMC1* complementary DNA was extremely challenging due to the low transcript abundance and high GC content. However, we were successful in sequencing 49.7% of the transcript (brown lines in Figure S4A). The retrieved sequences confirmed all the predicted exon-exon junctions, except for the exon 4/exon 5 junction that failed to amplify. The *Chlamydomonas* RNA-sequencing database (Oct.2007 Assembly) (Kent 2002;

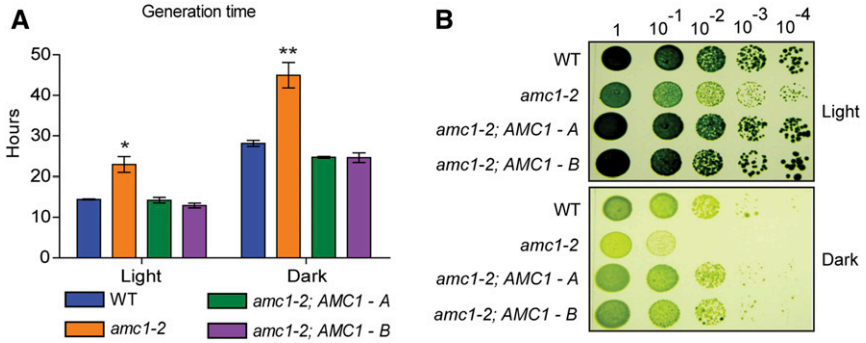

Figure 3 The SID phenotype of the *amc1-2* mutant is rescued by the wild-type *AMC1* gene. The growth phenotypes of wild-type (WT) (4C$^-$), *amc1-2* mutant, and the complemented strains [*amc1-2*; *AMC1-A*] and [*amc1-2*; *AMC1-B*], are compared here by studying growth on liquid and solid media. (A) The average generation time for each strain, determined from the growth curves in Figure S3B, is indicated here. The error bars represent SD of the mean. The two-tailed unequal variances *t*-test revealed a significant increase in the generation time of *amc1-2* with respect to WT, in the light and in the dark. In addition, the rescue of generation time in the dark was also significant for the complemented strains compared to the *amc1-2* mutant with a $P < 0.01$. * $P < 0.05$ and ** $P < 0.01$. (B) Restoration of the growth phenotype in the two [*amc1-2*; *AMC1*] complemented strains was confirmed by 10-fold dilution series, plated on acetate-containing medium and incubated in the light and in the dark for 12 days.

Karolchik *et al.* 2003; Blaby *et al.* 2014) corroborates the exon 4/exon 5 junction. From these results, we inferred that the coding sequence predicted by the JGI v5.5 is reliable.

The AMC1 protein sequence does not possess any recognizable domains indicating a possible function. If AMC1 plays a role in complex I biogenesis, it is highly plausible that mitochondrial localization is required for its function. Mitochondrial targeting is usually facilitated by a 10–80 amino-acid-long N terminal targeting sequence which forms an amphiphilic α-helix (von Heijne 1986; Habib *et al.* 2007). Algorithms have been designed to predict N terminal mitochondrial targeting peptides from protein sequences. Mitochondrial targeting of AMC1 was predicted by the TargetP, MitoFates, and PredAlgo algorithms (Emanuelsson *et al.* 2000; Tardif *et al.* 2012; Fukasawa *et al.* 2015).

We experimentally tested whether the N terminus of AMC1 can act as a mitochondrial targeting sequence by using a simple heterologous expression system with the UbiG reporter protein (Figure 5A). The *E. coli* UbiG and the *S. cerevisiae* Coq3 are proteins involved in ubiquinone biosynthesis. In *S. cerevisiae*, mitochondrial ubiquinone biosynthesis is essential for respiratory growth. It has been shown that *E. coli* UbiG can functionally complement the Δ*coq3* yeast mutant if UbiG is specifically targeted to the mitochondria with an appropriate targeting signal (Hsu *et al.* 1996). We utilized this heterologous system to test whether the AMC1 N terminus can target *E. coli* UbiG to yeast mitochondria and restore respiration. For this purpose, a construct was created containing the sequence encoding the first 59 amino acids of AMC1, fused to the 5′-end of the coding sequence of the *ubiG* gene (Figure 5B). The *ubiG* gene expressed without a mitochondrial targeting sequence failed to restore respiration (Hsu *et al.* 1996). Accordingly, we observed significantly decreased respiratory growth of the Δ*coq3* strain expressing *ubiG*. On the contrary, UbiG fused with the COQ3 mitochondrial targeting sequence or the first 59 amino acids of the AMC1 N-terminal sequence rescued respiratory growth of the Δ*coq3* mutant (Figure 5C). From these results, we conclude that the AMC1 N terminal sequence is capable of targeting a reporter protein to the yeast mitochondria. Hence, AMC1 likely localizes in the *Chlamydomonas* mitochondria by virtue of its N terminal sequence and functions in this compartment.

Loss of AMC1 results in decreased mitochondrial transcript abundance

Loss of AMC1 results in the accumulation of a 700 kDa membrane-bound subcomplex, a hallmark of mutants for the mitochondrial *nd4* and *nd5* genes whose products are part of the distal membrane arm (Remacle *et al.* 2006; Cardol *et al.* 2008). Hence, we hypothesized that AMC1 could control the mitochondrial synthesis of ND4 or ND5 subunits, and/or their assembly into the membrane arm. The mitochondrial genome of *Chlamydomonas* contains 13 intronless genes, of which eight encode for proteins (Figure 6A): *cob* (apocytochrome *b*, subunit of complex III); *cox1* (subunit 1 of complex IV); *nd1*, *nd2*, *nd4*, *nd5*, *nd6* (subunits of complex I); and *rtl* (reverse-transcriptase like protein) (Larosa and Remacle 2013). The genome is transcribed in a bi-directional manner, generating the left and right transcriptional units (LTU and RTU, respectively) (Gray and Boer 1988). The transcription start sites are predicted to be located between the genes *nd5* and *cox1* (Salinas-Giegé *et al.* 2017). The LTU is produced by the cotranscription of the *nd5*, *nd4*, and *cob* genes (Boer and Gray 1986; Gray and Boer 1988), which are later processed to individual transcripts. The RTU is generated by the cotranscription of the five protein-coding genes (*cox1*, *nd2*, *nd6*, *nd1*, and *rtl*), three transfer RNAs, and ribosomal RNAs (Figure 6, A and B), which are also processed into individual transcripts (Boer and Gray 1991). The mature transcripts begin at the start codon and do not have a 5′-UTR (Salinas-Giegé *et al.* 2017). This is similar to protein-encoding mitochondrial transcripts starting directly at the initiation codon in several organisms, such as humans (Rackham *et al.* 2012) and fission yeast (Herrmann *et al.* 2013; Kehrein *et al.* 2013), where the ribosomes display a clear preference for translation initiation on 5′-UTR-less transcripts (Christian and Spremulli 2010). In contrast, the 5′-UTR sequence plays an important role in the recognition of transcript by *S. cerevisiae* mitochondrial ribosomes (Lasserre *et al.* 2015). A newly discovered feature of the *Chlamydomonas* mitochondrial transcripts is

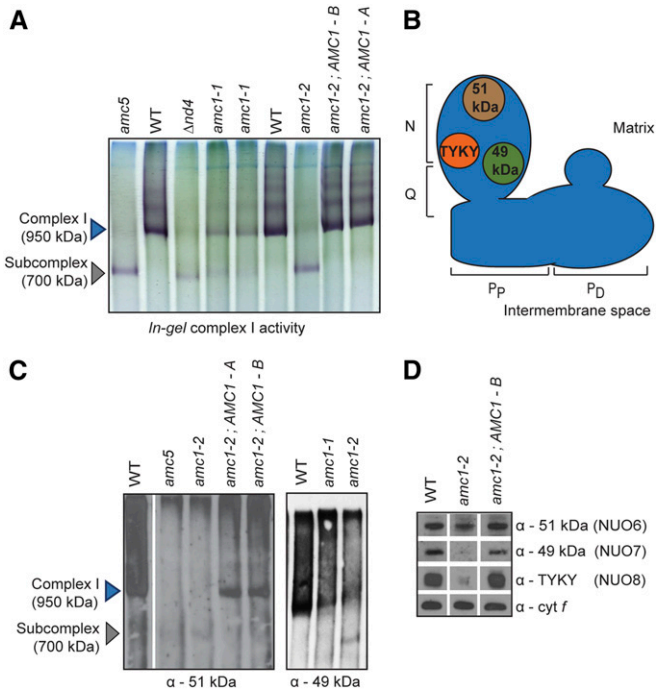

Figure 4 Complex I assembly is restored in the *amc1-2* mutant upon introduction of the *AMC1* gene. (A) BN-PAGE was conducted on 200 μg of partially purified membrane fraction. *In-gel* complex I activity was detected by NBT staining. The *amc1-2* mutant accumulates a labile 700 kDa subcomplex, similar to the *amc5* mutant and Δ*nd4* mutant. The *amc1-1* mutant strains also accumulate trace levels of the 700 kDa subcomplex, in addition to a full complex. Two *amc1-1* strains, original *amc1* (4C10) (lane 4) and the haploid progeny *amc1(2)* (lane 5) were tested. (B) An illustration of complex I structure depicting the locations of the immunodetected subunits of the matrix arm, which consists of the NADH-oxidizing N module and the quinone-binding Q module. The proton-pumping membrane arm is divided into the proximal (P_P) and distal (P_D) modules. (C) Immunoblotting using anti-51 kDa or anti-49 kDa antibody, of complexes separated by BN-PAGE. Two hundred micrograms of protein were loaded per lane. The white vertical line depicts that the WT is from a different lane of the same immunoblot. The *amc1(2)* strain carrying *amc1-1* allele was tested in the right panel. (D) SDS-PAGE immunoblotting was conducted on 10 μg of partially purified membranes using polyclonal antibodies to detect soluble arm complex I subunits α- 49 kDa, α- 51 kDa, and α- TYKY. α-cyt *f* was used as a loading control. The white vertical lines indicate assembly of different lanes from the same immunoblot. In A, C, and D, one representative of three biological replicates is shown. The *amc1-2* strain *amc11 (10G11)* and its corresponding complemented strains were tested here. WT, wild type.

the presence of polycytidylation at the 3′-end (Salinas-Giegé *et al.* 2017; Gallaher *et al.* 2018).

First, we tested if the abundance of mitochondrial DNA was affected by the loss of AMC1. Real-time quantitative PCR analysis on purified genomic DNA demonstrated that there was no significant change in the mitochondrial DNA content in the *amc1-1* and *amc1-2* mutants, relative to wild type (Figure 6C).

To test if the complex I dysfunction by the loss of AMC1 is due to defects in the expression of the mitochondrial genes encoding complex I subunits, we assessed the abundance of the mitochondrial protein-coding transcripts by real-time quantitative RT-PCR analysis (Figure 6, D and E). The *amc1-1* and the *amc1-2* mutants displayed increased levels of the *nd5* transcript of the LTU compared to the wild-type (twofold and 1.6-fold for *amc1-1* and *amc1-2*, respectively). On the contrary, a twofold decrease in the *nd4* transcript was observed in both the mutants. Upon complementation with the wild-type *AMC1* gene, the *nd5* and *nd4* transcripts were restored to wild-type levels, indicating that the abundance of the LTU transcripts encoding ND5 and ND4 is dependent upon AMC1. Since the abundance of the *nd5* and *cob* transcripts of the LTU was not decreased, we can rule out an attenuation in the transcription of the LTU as the cause of the decrease in the *nd4* transcript levels.

In the RTU, while the *amc1-2* mutant displayed no significant difference in the *nd6* and *nd1* transcript levels, both the *amc1-1* and *amc1-2* mutants showed a 1.4- to 1.5-fold decrease in the *nd2* transcripts, respectively. In addition, the *amc1-1* mutant also displayed a twofold down-accumulation of the *nd1* transcript. Finally, the *rtl* transcript levels were increased by 4.8-fold and fivefold, in the *amc1-2* and *amc1-1* mutants, respectively. The *cox1* and *rtl* transcripts were not down-accumulated in the mutants, underscoring that the transcription of the RTU is also not negatively affected. In summary, the *amc1-1* and *amc1-2* mutants displayed a decrease in the *nd4* and *nd2* transcript levels. The *amc1-1* mutant additionally displayed a decrease in the *nd1* transcript.

While our premise hypothesizes the decrease in the *nd* transcripts is due to loss of AMC1, it is possible that the mitochondrial transcript abundance is systematically affected as a consequence of complex I deficiency. To test this hypothesis, we assessed the mitochondrial transcript abundance in the *amc5* mutant (Figure S6). This mutant contains an insertional mutation in the nuclear *NUOB10* gene that encodes an accessory subunit located in the distal membrane arm of complex I (Barbieri *et al.* 2011; Zhu *et al.* 2015; Subrahmanian *et al.* 2020). The *amc5* mutant was chosen for comparison because it is another nuclear mutant that is characterized by a distal membrane arm assembly defect, similar to the *amc1-1* and *amc1-2* mutants (Figure 4A).

In the *amc5* mutant, there was no decrease in the levels of the LTU transcripts. Interestingly, a 2.9-fold increase was observed for the *nd5* transcript, similar to the *amc1-1* and *amc1-2* mutants, which was restored to wild-type levels upon complementation with the wild-type *NUOB10* gene (Figure S6). Contrary to the *amc1-1* and *amc1-2* mutants, a 1.5-fold increase in the *nd4* transcript was observed in the *amc5* mutant.

In the RTU, the *rtl* transcript level was also increased in the *amc5* mutant similar to the *amc1-1* and *amc1-2* mutants. In addition, the three *nd* transcript levels (*nd2*, *nd6*, *nd1*) were decreased and were restored upon complementation. The decrease in the *amc5* strain for the *nd2* and *nd1* transcripts is similar to the *amc1-1* and *amc1-2* mutants. However, based on their localization in the proximal membrane arm of complex I, complete loss of ND6, ND2, or ND1 is unlikely as this would result in a failure to assemble the 700 kDa subcomplex (Remacle *et al.* 2001a; Cardol *et al.* 2002).

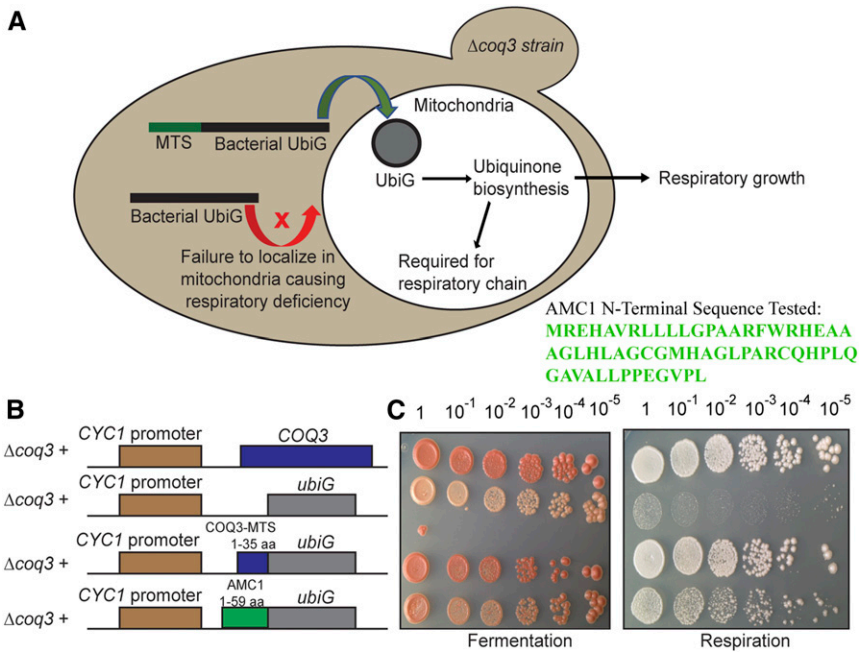

Figure 5 The N terminus of AMC1 targets the reporter protein UbiG to the yeast mitochondria. (A) A simple model illustrating the heterologous system of expression for testing the mitochondrial targeting signal. In a *S. cerevisiae* Δ*coq3* mutant deficient for ubiquinone biosynthesis, production of the bacterial ortholog UbiG restores ubiquinone synthesis if it is specifically targeted to the mitochondria by virtue of a mitochondrial targeting signal (MTS). The N-terminal sequence of AMC1 that was tested is displayed in green font. (B) Simplified representation of the inserts carried by the different plasmids used. The construction of the plasmids is described in Method S7. (C) The respiratory deficient Δ*coq3* mutant was transformed with constructs producing the UbiG reporter as a translational fusion with the first 59 aa in the N terminus of AMC1. The Δ*coq3* mutant transformed with the wild-type yeast *COQ3* gene, the *ubiG* gene lacking a MTS encoding sequence, and the *ubiG* gene with the sequence encoding the *COQ3* MTS were used as controls. Ten-fold serial dilutions were conducted on one representative transformant, plated on solid fermentable and respiratory media, and incubated at 28° for 7 days.

Most importantly, the significant decrease in the *nd4* transcript, observed in both the *amc1-1* and *amc1-2* mutants, is not a feature of the *amc5* mutant. From these results, we can conclude that loss of AMC1 specifically affects the abundance of the *nd4* transcript. Previous studies on mitochondrial mutants of *Chlamydomonas* have revealed that loss of ND4 results in the accumulation of a 700 kDa subcomplex (Remacle *et al.* 2001a, 2006), similar to the phenotype observed in the *amc1-1* and *amc1-2* mutants. Hence, we propose that the assembly defect resulting in the formation of the 700 kDa subcomplex in the *amc1-1* and the *amc1-2* mutants is due to a primary defect in the expression of the mitochondrial gene *nd4*.

Discussion

In this paper, we report the identification of a previously unrecognized player in *Chlamydomonas* complex I biogenesis. We have shown that (1) two allelic mutants exhibiting complex I deficiency, *amc1-1* and *amc1-2*, accumulate a 700 kDa subcomplex, diagnostic of an arrest in the assembly of the distal membrane arm of complex I; (2) both mutants carry insertional mutations in the unexplored *AMC1* gene; (3) complementation of the *amc1-2* mutant with the wild-type *AMC1* gene restores assembly and activity, thereby confirming the role of AMC1 in complex I function; (4) the N terminus of AMC1 is capable of targeting a reporter protein to the mitochondria; and (5) loss of AMC1 results in decreased steady-state levels of the mitochondrial *nd4* transcript.

AMC1 is required for the assembly of the distal membrane arm of complex I

The multimeric complex I consists of three major functional modules: (1) the NADH-binding N module; (2) the quinone-binding Q module, both part of the matrix-exposed peripheral arm; and (3) the proton-pumping P module of the membrane arm (Figure 4B and Figure 6B) (Mimaki *et al.* 2012). The P module is further subdivided based on location with respect to the peripheral arm into the proximal (P_P) and the distal (P_D) ends of the membrane arm. Complex I biogenesis requires the synthesis of >40 subunits followed by their precise step-wise integration into assembly intermediates to form the fully functional holoenzyme (Vogel *et al.* 2007). In instances where complex I biogenesis proceeds to form normal levels of active holoenzyme, the assembly intermediates are normally so transient that they can hardly be detected by electrophoretic methods. The loss of a subunit or a biogenesis factor affects the assembly process, blocking the formation of the mature complex and resulting in the accumulation of assembly intermediates. The study of complex I mutants in various model systems has revealed the occurrence of specific soluble and membrane-bound intermediates stalled at particular stages of assembly, enabling to delineate the precise order of complex I assembly in each organism (Videira and Duarte 2002; Radermacher *et al.* 2006; Mimaki *et al.* 2012; Subrahmanian *et al.* 2016; Formosa *et al.* 2018).

In this article we have reported two allelic insertional mutants, *amc1-1* and *amc1-2*, accumulating a ~700 kDa subcomplex (Figure 4). While multiple assembly intermediates have been identified in vascular plants and animals [reviewed in Subrahmanian *et al.* (2016), Guerrero-Castillo *et al.* (2017), Formosa *et al.* (2018), Ivanova *et al.* (2019)], only the ~700 kDa subcomplex has been well documented in *Chlamydomonas*. This assembly intermediate is a membrane-bound subcomplex which has been previously observed in mutants lacking the subunits of the P_D module, such as ND4, ND5, and NUOB10 (Cardol *et al.* 2002, 2008; Remacle *et al.* 2006; Barbieri *et al.* 2011; Massoz *et al.* 2017). It can be detected by *in-gel* NADH/NBT staining,

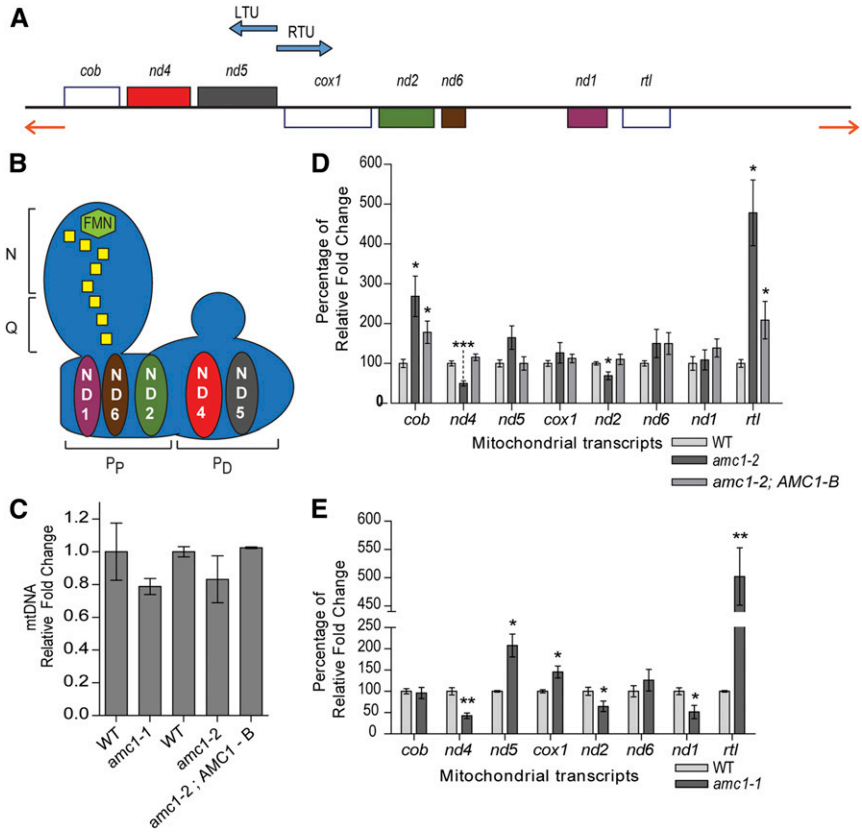

Figure 6 Loss of AMC1 results in decreased accumulation of the *nd4* transcript. (A) Simplified map of the 15.8 kb mitochondrial genome of *C. reinhardtii*, adapted from Larosa and Remacle (2013). The rectangles represent the eight protein-coding genes. The orange arrows represent the terminal inverted repeats. The blue arrows indicate the direction of transcription. The LTU contains *cob*, encoding the complex III subunit apocytochrome *b*; and *nd4* and *nd5*, encoding the complex I subunits ND4 and ND5, respectively. The RTU contains *cox1*, encoding subunit I of complex IV; *nd2*, *nd6*, and *nd1*, encoding the corresponding complex I subunits; and *rtl*, encoding a reverse-transcriptase like protein. (B) Simplified representation of L-shaped mitochondrial complex I embedded in the inner mitochondrial membrane. The flavin mononucleotide molecule is indicated in green and the Fe-S clusters are represented in yellow. The matrix arm consists of the NADH-oxidizing N module and the quinone-binding Q module. The proton-pumping membrane arm is divided into the proximal (P_P) and distal (P_D) modules. The putative locations of the mitochondrially encoded subunits of the membrane arm of complex I are represented here. (C) Real-time quantitative PCR was used to assess the relative quantity of mitochondrial DNA. The mitochondrial *nd4* gene was used as a target gene and the nuclear gene *TUA2*, encoding the alpha tubulin 2 protein, was used as the reference gene. The average was obtained from two biological replicates, each including three technical replicates, and the error bars represent SD of the mean. The results are represented as fold change relative to WT (WT set to 1.0). The *amc1-1* strain tested in C and E was *amc1 (4C10)* strain. The *amc1-2* strain tested in C and D was *amc11 (10G11)* strain. (D and E) Real-time quantitative RT-PCR was used to assess the relative abundance of the mitochondrial protein-coding transcripts, which was determined with respect to the geometric mean of three reference messenger RNAs *TUA2*, *EIF1A*, and *CBLP*. The average was obtained from three biological replicates each analyzed in two technical replicates. The results are represented as percentage of fold change relative to WT (WT set to 100). Statistical significance was determined by two-tailed unequal variances *t*-test. * $P < 0.05$, ** $P < 0.01$, *** $P < 0.001$. WT, wild type.

indicating that it consists of a functional peripheral arm capable of NADH dehydrogenase activity. Accordingly, proteomic analysis of the mitochondrial *nd5*-null mutant revealed the presence of at least 16 complex I subunits in the 700 kDa subcomplex (Cardol *et al.* 2008). This includes the seven core subunits from the N- and Q- modules required for NADH dehydrogenase activity, and the P_p module allowing the subcomplex to attach to the membrane. However, it lacks subunits of the P_D module required for a firm anchoring to the membrane, further highlighting this subcomplex does not contain the distal membrane arm of complex I. Since the 700 kDa subcomplex is loosely anchored to the mitochondrial inner membrane, it is highly labile and its detection in membrane fractions varies with each extraction (Figure 4) (Barbieri *et al.* 2011). In addition to the 700 kDa subcomplex, lower amounts of mature complex I are present in the *amc1-1* and *amc1-2* mutants indicating that limited membrane arm assembly can still occur in the absence of wild-type *AMC1* (Figure 4 and Figure S5).

Structural features of the AMC1 protein

AMC1 is a large protein of 2566 residues with an expected molecular mass of 254 kDa. It is annotated in the *Chlamydomonas* genome database as a hypothetical protein (*Cre16.g688900*) and does not exhibit any significant sequence homology to proteins from bacteria, fungi, land plants, or animals. Heterologous expression in yeast has revealed that the first 59 amino acids of the AMC1 N terminus are sufficient to target a functional reporter protein to yeast mitochondria (Figure 5). From these results, we infer that AMC1 localizes to the *Chlamydomonas* mitochondria where it functions in complex I biogenesis.

The AMC1 sequence is enriched for low-complexity regions, which are regions of biased amino acid composition. In AMC1, the predominant amino acids are Ala (24.2%), Gly (11.3%), Leu (9.9%), and Pro (7.1%) (Figure 7A). This feature is present in several nuclear-encoded Pentatrico Peptide Repeat (PPR) and Octotrico Peptide Repeat (OPR) proteins known to control the processing, splicing, editing, stabilization, and translation of transcripts in mitochondria and plastids (Boulouis *et al.* 2011; Barkan and Small 2014; Cline *et al.* 2017; Viola *et al.* 2019). PPRs and OPRs are defined by tandemly repeated motifs with degenerate amino acid sequences forming α-helical repeats that bind a target nucleotide sequence (Rahire *et al.* 2012; Manna 2015). However, PPR or OPR motifs are not detected in AMC1. Yet, additional features similar to organellar RNA-interacting proteins are present

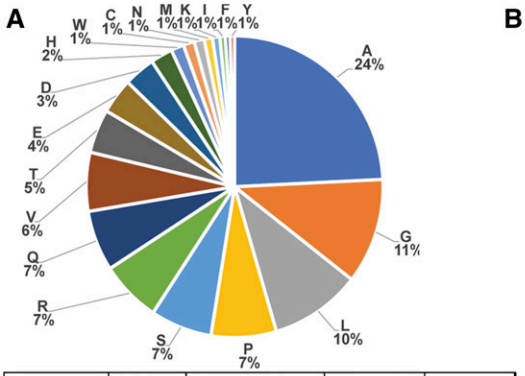

Type of residue	Amino acid name	Number of occurences in protein sequence	Percentage of occurrence	Ranking based on prevalence
Non-polar	Ala (A)	621	24.20%	1
	Gly (G)	289	11.30%	2
	Leu (L)	255	9.90%	3
	Pro (P)	182	7.10%	4
	Val (V)	162	6.30%	8
	Trp (W)	36	1.40%	13
	Met (M)	22	0.90%	16
	Ile (I)	16	0.60%	18
	Phe (F)	14	0.50%	19
Polar, non-charged	Ser (S)	173	6.70%	5
	Gln (Q)	166	6.50%	7
	Thr (T)	121	4.70%	9
	Cys (C)	32	1.20%	14
	Asn (N)	29	1.10%	15
	Tyr (Y)	12	0.50%	20
Polar, charged	Arg (R)	170	6.60%	6
	Glu (E)	97	3.80%	10
	Asp (D)	86	3.40%	11
	His (H)	62	2.40%	12
	Lys (K)	21	0.80%	17

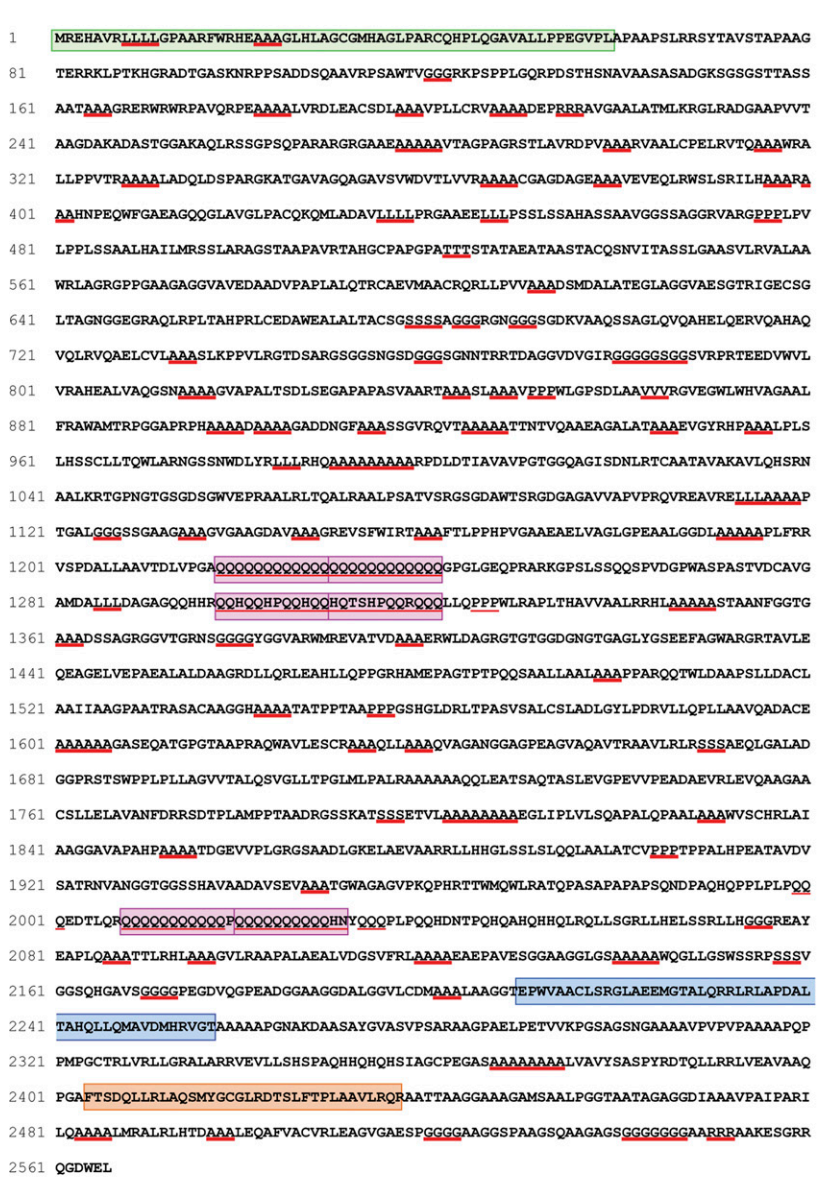

Figure 7 AMC1 is a low-complexity protein with polyQ regions. (A) Amino acid composition of AMC1 is depicted as a percentage of total number of residues in the form of a pie chart for easy visual representation (top panel) and also as a table classifying the amino acids based on the properties of their side groups (bottom panel). The top five prevalent residues Ala, Gly, Leu, Pro, and Ser, are represented in red font in the table. (B) Amino acid sequence of AMC1. Any amino acid stretches that are three or more residues long, with polyA, polyQ, and polyG as the most prevalent, are indicated by a red underline. The MEME algorithm recognized a polyQ motif represented in pink boxes, the consensus sequence for which is shown in C. The green box indicates the first 59 amino acids fused to the ubiG reporter in Figure 5. The blue and orange boxes depict the sequences of the motifs 1 and 2, respectively, in AMC1 that were identified by MEME to have similarity within the C-termini of the *Volvox* and *Gonium* AMC1-like proteins. The consensus sequence for motifs 1 and 2 are provided in Figure S7. (C) WebLogo consensus sequence of the polyQ motif identified by the MEME program (Bailey *et al.* 2009). The letter height represents the probability of a particular amino acid at that position (*y*-axis) within the 12 amino acid repeat (*x*-axis).

in AMC1. First, like the chloroplast PPR and OPR proteins of *Chlamydomonas*, AMC1 contains stretches of amino acid repeats, predominantly alanine, glutamine, glycine, leucine, and proline (Figure 7B). Low-complexity proteins with polyalanine repeats have been well documented to have roles in transcriptional regulation, either through DNA- or RNA-binding capacity (Radó-Trilla and Albà 2012). In addition, six internally repeated polyQ (poly-glutamine) motifs with histidine and proline interruptions have been recognized by the MEME algorithm (Figure 7C) (Bailey *et al.* 2009), and matches to multiple OPRs (Wostrikoff *et al.* 2001; Auchincloss *et al.* 2002; Rahire *et al.* 2012; Marx *et al.* 2015; Viola *et al.* 2019). Interestingly, histidine and proline interruptions in the polyQ stretches were shown to decrease the tendency for polyQ motifs to aggregate by providing higher solubility (Sen *et al.* 2003). PolyQ sequences are associated with various processes including transcriptional regulation and RNA binding (Schaefer *et al.* 2012).

Second, the large size of the protein (2566 residues) is a common feature of *Chlamydomonas* PPR and OPR proteins involved in chloroplast gene expression, the majority of which are >1000 residues in length (Boulouis *et al.* 2011; Rahire *et al.* 2012). Third, α-helical structures that are also a prominent feature in organellar RNA-interacting proteins (Boulouis *et al.* 2015), are predicted with high confidence and good correlation for AMC1 by Phyre2, Porter, and PSIPRED (Pollastri and McLysaght 2005; Buchan *et al.* 2013; Kelley *et al.* 2015). Finally, Phyre2, PSIPRED, and IUPRED also predicted multiple disordered regions, as expected from the presence of low-complexity regions in AMC1 (Dosztányi *et al.* 2005a,b; Buchan *et al.* 2013; Kelley *et al.* 2015). Through their conformational variability and adaptability, disordered regions can support diverse functions such as scaffolding and recruitment of interacting partners (van der Lee *et al.* 2014).

From these similarities to proteins involved in the regulation of gene expression, we hypothesize that AMC1 may have a primary function in mitochondrial gene expression. We propose that AMC1 may directly bind RNA or may regulate gene expression by interacting with other RNA-binding proteins.

AMC1 is required for the expression of the mitochondrial nd4 transcript

Analysis of mitochondrial transcripts has shown that loss of AMC1 results in a decreased accumulation of the *nd4* transcript, which was restored upon complementation (Figure 6). However, this defect was not observed in the *nuob10*-null mutant (Figure S6) even though it was also deficient in the assembly of the distal membrane arm (Figure 4A). Since decreased levels of *nd4* transcript were specifically reproduced in both the *amc1-1* and *amc1-2* mutants, it is most likely that AMC1 functions in complex I biogenesis through its involvement in *nd4* gene expression.

The *nd4* transcript levels could be diminished due to (1) decreased transcription, and/or (2) increased degradation of the *nd4* transcript. The *nd4* transcript is synthesized as part of the polycistronic LTU and then processed to form the individual transcript for translation (Gray and Boer 1988). However, the levels of the *nd5* and *cob* transcripts, which are also part of the LTU, are not decreased in *amc1-1* and *amc1-2* (Figure 6C). Hence, we conclude that the problem does not lie with the transcription of the *nd4* gene.

A second possibility is that while the LTU is transcribed normally, it is not processed to release the individual transcripts for translation. However, we do not observe any associated decrease in *cob* and *nd5* transcript levels due to loss of processing or a resultant complex III deficiency in the *amc1-1* or *amc1-2* mutants (Figure 2B and Barbieri *et al.* 2011; Subrahmanian *et al.* 2020). This indicates that *cob* is translated and thereby processed normally and we can conclude that processing of the LTU is likely not affected.

A simple hypothesis to account for the assembly defect in the distal arm is a loss of ND4 and/or ND5. Based on the fact that the abundance of the *nd4* transcript is reduced but not that of *nd5*, we hypothesize that the AMC1-dependent assembly defect is primarily due to loss of ND4.

It is plausible that AMC1 functions in stabilizing the *nd4* transcript based on the fact that in the *amc1-1* and *amc1-2* mutants the *nd4* transcript accumulates to ∼42 and ∼50% of wild-type, respectively. However, organellar transcript levels may not be rate-limiting. In the chloroplast, transcripts can be reduced to <10% of wild type by chemical treatment and the rate of translation still remains largely unaffected (Choquet and Wollman 2002). In the *Chlamydomonas* mitochondria, a single deletion in the 3′-UTR of the *nd5* transcript still allows for the accumulation of the mature complex to 17% of wild-type levels, despite a drastic decrease in the mature *nd5* transcript levels (Cardol *et al.* 2002). Although the stability of the *nd5* transcript was severely affected by the 3′-UTR mutation, a 700 kDa subcomplex was not detected in this mutant, indicating that the synthesis of ND5 and the assembly of the distal membrane arm were not significantly affected to result in the accumulation of the 700 kDa subcomplex (Cardol *et al.* 2002). In the *amc1-1* and *amc1-2* mutants, the *nd4* transcript abundance is reduced only by twofold but a 700 kDa subcomplex is detected, implying that the transcript levels may not be rate-limiting. We favor a model in which the primary defect due to loss of AMC1 function lies in the synthesis and assembly of ND4 into the distal arm. It must be noted that a complete lack of ND4 due to the loss of AMC1 is unlikely as traces of mature complex I are formed, in addition to the 700 kDa subcomplex (Figure 4 and Figure S5). Hence, we propose that loss of AMC1 function severely affects, but does not completely abolish, ND4 synthesis.

At the present time, the mode of action of AMC1 is speculative, but based on our results, we favor the hypothesis that AMC1 is primarily involved in translation of the *nd4* transcript. To account for the downaccumulation of the *nd4* transcript in the *amc1-1* and *amc1-2* mutants, we hypothesize that loss of ND4 synthesis may have a secondary effect on the *nd4* transcript stability, resulting in twofold decrease of the relative *nd4* transcript levels. However, it is also conceivable that AMC1 has dual function and controls both the stability and the translation of the *nd4* transcript. Based on the features of the protein sequence, the function(s) of AMC1 may be executed either through direct RNA binding or through interactions with other RNA-binding proteins. Future investigations would involve documenting the effect of loss of AMC1 on mitochondrial translation. However, the tools currently available for investigating mitochondrial translation in *Chlamydomonas* are limited. Although a preliminary *in organello* translation study was reported, the pattern of migration of all the labeled polypeptides could not be definitively correlated with the expected gene products (Salinas *et al.* 2012). In addition, antibodies to detect the steady-state abundance of *Chlamydomonas* mitochondrial ND proteins are not available and our several attempts to detect the ND4 protein with antibodies against *Arabidopsis* Nad4 (PhytoAB Inc.) and *Polytomella* Nad4 (a generous gift from D. Gonzalez-Halphen) were unsuccessful (data not shown).

The ND4 subunit, consisting of 443 residues that form 14 conserved transmembrane helices, is involved in proton translocation (Efremov *et al.* 2010; Efremov and Sazanov 2011). Mitochondrially-encoded proteins are known to be cotranslationally inserted into the inner mitochondrial membrane (Ott and Herrmann 2010). Proteins assisting this process in *Chlamydomonas* remain unidentified. At this point, we cannot rule out that AMC1 may be involved in cotranslational insertion of ND4 in the membrane or post-translational chaperoning of ND4 to facilitate its integration in complex I.

A defect in membrane arm assembly due to loss of mitochondrially-encoded ND4 has also been reported in plants and human cells (Hofhaus 1993; Karpova 1999). Although it is one of the core subunits, *Chlamydomonas* ND4 has only 27 and 39% sequence identity with mammalian and tobacco ND4, respectively, indicating a higher evolutionary distance between ND4 of various species (Ma *et al.* 1989; Pratje *et al.* 1989). Such evolutionary changes in the protein sequence would necessitate coevolution of the factors responsible for regulating the expression of the corresponding mitochondrial transcript (Costanzo *et al.* 2000). Hence, it is conceivable that proteins involved in *Chlamydomonas* mitochondrial gene expression have also accrued modifications and features to accommodate the corresponding changes in their target transcripts. Consistent with this view is the fact that AMC1-like proteins can only be detected in other green algae such as *Volvox carteri* and *Gonium pectorale*, which are close relatives of *Chlamydomonas* (Figure S7). Interestingly, the AMC1-like proteins from *Volvox* and *Gonium* are also low-complexity proteins with polyG, polyS, and polyP stretches. In addition, the *Volvox* protein harbors two short polyQ motifs. Note that the similarity is limited to the C terminus, an indication that this domain is probably important for the function of the AMC1-like proteins. A common feature of the three proteins is the presence of two partially degenerated motifs separated by 137–214 residues at the C-terminal end (Figure 7 and Figure S7). The two motifs are 48 and 34 residues in length. A common C-terminal motif in three algal counterparts might be indicative of a conserved algal domain with a common function. Further experiments are required to elaborate the mechanism of action of AMC1.

In conclusion, we have utilized a forward genetic screen in *C. reinhardtii* to reveal a novel nuclear-encoded factor involved in mitochondrial gene expression and required for complex I biogenesis. This study opens new avenues of exploration to delineate the processes of mitochondrial gene expression and their role in mitochondrial function.

Acknowledgments

We thank Amrita Saha, Quentin Nickerson, Elizabeth Zebrowski, Clara Bredow, and Femke Ehlers for their technical assistance in the laboratory. We thank Rebecca Davis and Pallavi Chandna for careful proofreading of the manuscript. We are grateful to Catherine Clark (University of California, Los Angeles) for her kind gifts of strains and plasmids. We also thank the University of Liège for providing a collaborative research fellowship to N.S. C.R. acknowledges support from Fonds de la Recherche Scientifique (CDR J.0265.17 and J.0175.20). This research was supported by a grant from the United Mitochondrial Disease Foundation (to P.P.H. and C.R.) and a Centrer for Applied Plant Sciences grant (to P.P.H). The authors declare that there is no conflict of interest.

Literature Cited

Asamizu, E., K. Miura, K. Kucho, Y. Inoue, H. Fukuzawa *et al.*, 2000 Generation of expressed sequence tags from low-CO2 and high-CO2 adapted cells of Chlamydomonas reinhardtii. DNA Res. 7: 305–307. https://doi.org/10.1093/dnares/7.5.305

Auchincloss, A. H., W. Zerges, K. Perron, J. Girard-Bascou, and J. D. Rochaix, 2002 Characterization of Tbc2, a nucleus-encoded factor specifically required for translation of the chloroplast psbC mRNA in Chlamydomonas reinhardtii. J. Cell Biol. 157: 953–962. https://doi.org/10.1083/jcb.200201060

Bailey, T. L., M. Boden, F. A. Buske, M. Frith, C. E. Grant *et al.*, 2009 MEME SUITE: tools for motif discovery and searching. Nucleic Acids Res. 37: W202–W208. https://doi.org/10.1093/nar/gkp335

Baradaran, R., J. M. Berrisford, G. S. Minhas, and L. A. Sazanov, 2013 Crystal structure of the entire respiratory complex I. Nature 494: 443–448. https://doi.org/10.1038/nature11871

Barbieri, M. R., V. Larosa, C. Nouet, N. Subrahmanian, C. Remacle *et al.*, 2011 A forward genetic screen identifies mutants deficient for mitochondrial complex I assembly in *Chlamydomonas reinhardtii*. Genetics 188: 349–358. https://doi.org/10.1534/genetics.111.128827

Barkan, A., and I. Small, 2014 Pentatricopeptide repeat proteins in plants. Annu. Rev. Plant Biol. 65: 415–442. https://doi.org/10.1146/annurev-arplant-050213-040159

Blaby, I. K., C. E. Blaby-Haas, N. Tourasse, E. F. Hom, D. Lopez *et al.*, 2014 The Chlamydomonas genome project: a decade on. Trends Plant Sci. 19: 672–680. https://doi.org/10.1016/j.tplants.2014.05.008

Boer, P. H., and M. W. Gray, 1986 The URF 5 gene of *Chlamydomonas reinhardtii* mitochondria: DNA sequence and mode of transcription. EMBO J. 5: 21–28. https://doi.org/10.1002/j.1460-2075.1986.tb04172.x

Boer, P. H., and M. W. Gray, 1991 Short dispersed repeats localized in spacer regions of Chlamydomonas reinhardtii mitochondrial DNA. Curr. Genet. 19: 309–312. https://doi.org/10.1007/BF00355060

Boulouis, A., C. Raynaud, S. Bujaldon, A. Aznar, F. A. Wollman *et al.*, 2011 The nucleus-encoded trans-acting factor MCA1 plays a critical role in the regulation of cytochrome f synthesis in Chlamydomonas chloroplasts. Plant Cell 23: 333–349. https://doi.org/10.1105/tpc.110.078170

Boulouis, A., D. Drapier, H. Razafimanantsoa, K. Wostrikoff, N. J. Tourasse *et al.*, 2015 Spontaneous dominant mutations in chlamydomonas highlight ongoing evolution by gene diversification. Plant Cell 27: 984–1001. https://doi.org/10.1105/tpc.15.00010

Braun, H. P., S. Binder, A. Brennicke, H. Eubel, A. R. Fernie *et al.*, 2014 The life of plant mitochondrial complex I. Mitochondrion 19: 295–313. https://doi.org/10.1016/j.mito.2014.02.006

Buchan, D. W., F. Minneci, T. C. Nugent, K. Bryson, and D. T. Jones, 2013 Scalable web services for the PSIPRED protein analysis workbench. Nucleic Acids Res. 41: W349–W357. https://doi.org/10.1093/nar/gkt381

Cardol, P., R. F. Matagne, and C. Remacle, 2002 Impact of mutations affecting ND mitochondria-encoded subunits on the activity and assembly of complex I in *Chlamydomonas*. Implication

for the structural organization of the enzyme. J. Mol. Biol. 319: 1211–1221. https://doi.org/10.1016/S0022-2836(02)00407-2

Cardol, P., G. Gloire, M. Havaux, C. Remacle, R. Matagne *et al.*, 2003 Photosynthesis and state transitions in mitochondrial mutants of *Chlamydomonas reinhardtii* affected in respiration. Plant Physiol. 133: 2010–2020. https://doi.org/10.1104/pp.103.028076

Cardol, P., M. Lapaille, P. Minet, F. Franck, R. F. Matagne *et al.*, 2006 ND3 and ND4L subunits of mitochondrial complex I, both nucleus encoded in *Chlamydomonas reinhardtii*, are required for activity and assembly of the enzyme. Eukaryot. Cell 5: 1460–1467. https://doi.org/10.1128/EC.00118-06

Cardol, P., L. Boutaffala, S. Memmi, B. Devreese, R. F. Matagne *et al.*, 2008 In *Chlamydomonas*, the loss of ND5 subunit prevents the assembly of whole mitochondrial complex I and leads to the formation of a low abundant 700 kDa subcomplex. Biochim. Biophys. Acta 1777: 388–396. https://doi.org/10.1016/j.bbabio.2008.01.001

Chen, D. C., B. C. Yang, and T. T. Kuo, 1992 One-step transformation of yeast in stationary phase. Curr. Genet. 21: 83–84. https://doi.org/10.1007/BF00318659

Choquet, Y., and F. A. Wollman, 2002 Translational regulations as specific traits of chloroplast gene expression. FEBS Lett. 529: 39–42. https://doi.org/10.1016/S0014-5793(02)03260-X

Christian, B. E., and L. L. Spremulli, 2010 Preferential selection of the 5′- terminal start codon on leaderless mRNAs by mammalian mitochondrial ribosomes. J. Biol. Chem. 285: 28379–28386. https://doi.org/10.1074/jbc.M110.149054

Clarke, C. F., W. Williams, and J. H. Teruya, 1991 Ubiquinone biosynthesis in Saccharomyces cerevisiae. Isolation and sequence of COQ3, the 3,4-dihydroxy-5-hexaprenylbenzoate methyltransferase gene. J. Biol. Chem. 266: 16636–16644. https://www.jbc.org/content/266/25/16636.long

Cline, S. G., I. A. Laughbaum, and P. P. Hamel, 2017 CCS2, an octatricopeptide-repeat protein, is required for plastid cytochrome c assembly in the green alga chlamydomonas reinhardtii. Front. Plant Sci. 8: 1306. https://doi.org/10.3389/fpls.2017.01306

Costanzo, M. C., N. Bonnefoy, E. H. Williams, G. D. Clark-Walker, and T. D. Fox, 2000 Highly diverged homologs of Saccharomyces cerevisiae mitochondrial mRNA-specific translational activators have orthologous functions in other budding yeasts. Genetics 154: 999–1012. https://www.ncbi.nlm.nih.gov/pubmed/10757749

de Montaigu, A., E. Sanz-Luque, A. Galvan, and E. Fernandez, 2010 A soluble guanylate cyclase mediates negative signaling by ammonium on expression of nitrate reductase in Chlamydomonas. Plant Cell 22: 1532–1548. https://doi.org/10.1105/tpc.108.062380

Dorthu, M. P., S. Remy, M. R. Michel-Wolwertz, L. Colleaux, D. Breyer *et al.*, 1992 Biochemical, genetic and molecular characterization of new respiratory-deficient mutants in Chlamydomonas reinhardtii. Plant Mol. Biol. 18: 759–772. https://doi.org/10.1007/BF00020017

Dosztányi, Z., V. Csizmok, P. Tompa, and I. Simon, 2005a IUPred: web server for the prediction of intrinsically unstructured regions of proteins based on estimated energy content. Bioinformatics 21: 3433–3434. https://doi.org/10.1093/bioinformatics/bti541

Dosztányi, Z., V. Csizmók, P. Tompa, and I. Simon, 2005b The pairwise energy content estimated from amino acid composition discriminates between folded and intrinsically unstructured proteins. J. Mol. Biol. 347: 827–839. https://doi.org/10.1016/j.jmb.2005.01.071

Dudkina, N. V., H. Eubel, W. Keegstra, E. J. Boekema, and H. P. Braun, 2005 Structure of a mitochondrial supercomplex formed by respiratory-chain complexes I and III. Proc. Natl. Acad. Sci. USA 102: 3225–3229. https://doi.org/10.1073/pnas.0408870102

Dujardin, G., P. Pajot, O. Groudinsky, and P. P. Slonimski, 1980 Long range control circuits within mitochondria and between nucleus and mitochondria. I. Methodology and phenomenology of suppressors. Mol. Gen. Genet. 179: 469–482. https://doi.org/10.1007/BF00271736

Efremov, R. G., and L. A. Sazanov, 2011 Structure of the membrane domain of respiratory complex I. Nature 476: 414–420. https://doi.org/10.1038/nature10330

Efremov, R. G., R. Baradaran, and L. A. Sazanov, 2010 The architecture of respiratory complex I. Nature 465: 441–445. https://doi.org/10.1038/nature09066

Emanuelsson, O., H. Nielsen, S. Brunak, and G. von Heijne, 2000 Predicting subcellular localization of proteins based on their N-terminal amino acid sequence. J. Mol. Biol. 300: 1005–1016. https://doi.org/10.1006/jmbi.2000.3903

Fassone, E., A. J. Duncan, J. W. Taanman, A. T. Pagnamenta, M. I. Sadowski *et al.*, 2010 FOXRED1, encoding an FAD-dependent oxidoreductase complex-I-specific molecular chaperone, is mutated in infantile-onset mitochondrial encephalopathy. Hum. Mol. Genet. 19: 4837–4847 [corrigenda: Hum. Mol. Genet. 24: 4183 (2015)]. https://doi.org/10.1093/hmg/ddq414

Formosa, L. E., M. G. Dibley, D. A. Stroud, and M. T. Ryan, 2018 Building a complex complex: assembly of mitochondrial respiratory chain complex I. Semin. Cell Dev. Biol. 76: 154–162. https://doi.org/10.1016/j.semcdb.2017.08.011

Fukasawa, Y., J. Tsuji, S. C. Fu, K. Tomii, P. Horton *et al.*, 2015 MitoFates: improved prediction of mitochondrial targeting sequences and their cleavage sites. Mol. Cell. Proteomics 14: 1113–1126. https://doi.org/10.1074/mcp.M114.043083

Gallaher, S. D., S. T. Fitz-Gibbon, D. Strenkert, S. O. Purvine, M. Pellegrini *et al.*, 2018 High-throughput sequencing of the chloroplast and mitochondrion of Chlamydomonas reinhardtii to generate improved de novo assemblies, analyze expression patterns and transcript speciation, and evaluate diversity among laboratory strains and wild isolates. Plant J. 93: 545–565. https://doi.org/10.1111/tpj.13788

Gray, M. W., and P. H. Boer, 1988 Organization and expression of algal (*Chlamydomonas reinhardtii*) mitochondrial DNA. Philos. Trans. R. Soc. Lond. B Biol. Sci. 319: 135–147. https://royalsocietypublishing.org/doi/10.1098/rstb.1988.0038

Green, D. E., and A. Tzagoloff, 1966 The mitochondrial electron transfer chain. Arch. Biochem. Biophys. 116: 293–304. https://doi.org/10.1016/0003-9861(66)90036-1

Guerrero-Castillo, S., F. Baertling, D. Kownatzki, H. J. Wessels, S. Arnold *et al.*, 2017 The assembly pathway of mitochondrial respiratory chain complex I. Cell Metab. 25: 128–139. https://doi.org/10.1016/j.cmet.2016.09.002

Habib, S. J., W. Neupert, and D. Rapaport, 2007 Analysis and prediction of mitochondrial targeting signals. *Methods Cell Biol.* 80: 761–781. https://doi.org/10.1016/S0091-679X(06)80035-X

Harris, E. H., 1989 *The Chlamydomonas Sourcebook: A Comprehensive Guide to Biology and Laboratory Use*. Academic Press, San Diego. ISBN-13: 978-0123268808

Herrmann, J. M., M. W. Woellhaf, and N. Bonnefoy, 2013 Control of protein synthesis in yeast mitochondria: the concept of translational activators. Biochim. Biophys. Acta 1833: 286–294. https://doi.org/10.1016/j.bbamcr.2012.03.007

Hinkle, P. C., 2005 P/O ratios of mitochondrial oxidative phosphorylation. Biochim. Biophys. Acta 1706: 1–11. https://doi.org/10.1016/j.bbabio.2004.09.004

Hofhaus, G., and G. Attardi, 1993 Lack of assembly of mitochondrial DNA-encoded subunits of respiratory NADH dehydrogenase and loss of enzyme activity in a human cell mutant lacking the mitochondrial ND4 gene product. EMBO J. 12: 3043–3048. https://pubmed.ncbi.nlm.nih.gov/8344246-lack-of-assembly-of-mitochondrial-dna-encoded-subunits-of-respiratory-nadh-dehydrogenase-and-loss-of-enzyme-activity-in-a-human-cell-mutant-lacking-the-mitochondrial-nd4-gene-product/

Hsu, A. Y., W. W. Poon, J. A. Shepherd, D. C. Myles, and C. F. Clarke, 1996 Complementation of coq3 mutant yeast by mitochondrial targeting of the Escherichia coli UbiG polypeptide: evidence that UbiG catalyzes both O-methylation steps in ubiquinone biosynthesis. Biochemistry 35: 9797–9806. https://doi.org/10.1021/bi9602932

Ivanova, A., M. Gill-Hille, S. Huang, R. Branca, B. Kmiec *et al.*, 2019 A mitochondrial LYR protein is required for complex I assembly. Plant Physiol. 181: 1632–1650. https://doi.org/10.1104/pp.19.00822

Karolchik, D., R. Baertsch, M. Diekhans, T. S. Furey, A. Hinrichs *et al.*, 2003 The UCSC genome browser database. Nucleic Acids Res. 31: 51–54. https://doi.org/10.1093/nar/gkg129

Varpova, O. V., and K. J. Newton, 2002 A partially assembled complex I in NAD4-deficient mitochondria of maize. Available at: https://doi.org/10.1046/j.1365-313X.1999.00401.x. Accessed: November 11, 2019.

Kehrein, K., N. Bonnefoy, and M. Ott, 2013 Mitochondrial protein synthesis: efficiency and accuracy. Antioxid. Redox Signal. 19: 1928–1939. https://doi.org/10.1089/ars.2012.4896

Kelley, L. A., S. Mezulis, C. M. Yates, M. N. Wass, and M. J. Sternberg, 2015 The Phyre2 web portal for protein modeling, prediction and analysis. Nat. Protoc. 10: 845–858. https://doi.org/10.1038/nprot.2015.053

Kent, W. J., 2002 BLAT–the BLAST-like alignment tool. Genome Res. 12: 656–664. https://doi.org/10.1101/gr.229202

Kropat, J., A. Hong-Hermesdorf, D. Casero, P. Ent, M. Castruita *et al.*, 2011 A revised mineral nutrient supplement increases biomass and growth rate in Chlamydomonas reinhardtii. Plant J. 66: 770–780. https://doi.org/10.1111/j.1365-313X.2011.04537.x

Lapaille, M., A. Escobar-Ramírez, H. Degand, D. Baurain, E. Rodríguez-Salinas *et al.*, 2010 Atypical subunit composition of the chlorophycean mitochondrial F1FO-ATP synthase and role of Asa7 protein in stability and oligomycin resistance of the enzyme. Mol. Biol. Evol. 27: 1630–1644. https://doi.org/10.1093/molbev/msq049

Larosa, V., and C. Remacle, 2013 Transformation of the mitochondrial genome. Int. J. Dev. Biol. 57: 659–665. https://doi.org/10.1387/ijdb.130230cr

Lasserre, J. P., A. Dautant, R. S. Aiyar, R. Kucharczyk, A. Glatigny *et al.*, 2015 Yeast as a system for modeling mitochondrial disease mechanisms and discovering therapies. Dis. Model. Mech. 8: 509–526. https://doi.org/10.1242/dmm.020438

Lecler, R., H. Vigeolas, B. Emonds-Alt, P. Cardol, and C. Remacle, 2012 Characterization of an internal type-II NADH dehydrogenase from Chlamydomonas reinhardtii mitochondria. Curr. Genet. 58: 205–216. https://doi.org/10.1007/s00294-012-0378-2

Letts, J. A., and L. A. Sazanov, 2015 Gaining mass: the structure of respiratory complex I — from bacterial towards mitochondrial versions. Curr. Opin. Struct. Biol. 33: 135–145. https://doi.org/10.1016/j.sbi.2015.08.008

Ma, D. P., Y. W. Yang, Y. T. King, and S. E. Hasnain, 1989 Nucleotide sequence of cloned nad4 (urf4) gene from Chlamydomonas reinhardtii mitochondrial DNA. Gene 85: 363–370. https://doi.org/10.1016/0378-1119(89)90429-0

Manna, S., 2015 An overview of pentatricopeptide repeat proteins and their applications. Biochimie 113: 93–99. https://doi.org/10.1016/j.biochi.2015.04.004

Marx, C., C. Wunsch, and U. Kuck, 2015 The octatricopeptide repeat protein Raa8 is required for chloroplast trans splicing. Eukaryot. Cell 14: 998–1005. https://doi.org/10.1128/EC.00096-15

Massoz, S., M. Hanikenne, B. Bailleul, N. Coosemans, M. Radoux *et al.*, 2017 In vivo chlorophyll fluorescence screening allows the isolation of a Chlamydomonas mutant defective for NDUFAF3, an assembly factor involved in mitochondrial complex I assembly. Plant J. 92: 584–595. https://doi.org/10.1111/tpj.13677

Mimaki, M., X. Wang, M. McKenzie, D. R. Thorburn, and M. T. Ryan, 2012 Understanding mitochondrial complex I assembly in health and disease. Biochim. Biophys. Acta 1817: 851–862. https://doi.org/10.1016/j.bbabio.2011.08.010

Mitchell, P., 1966 Chemiosmotic coupling in oxidative and photosynthetic phosphorylation. Biol. Rev. Camb. Philos. Soc. 41: 445–502. https://doi.org/10.1111/j.1469-185X.1966.tb01501.x

Ott, M., and J. M. Herrmann, 2010 Co-translational membrane insertion of mitochondrially encoded proteins. Biochim. Biophys. Acta 1803: 767–775. https://doi.org/10.1016/j.bbamcr.2009.11.010

Peters, K., N. V. Dudkina, L. Jansch, H. P. Braun, and E. J. Boekema, 2008 A structural investigation of complex I and I+III2 supercomplex from Zea mays at 11–13 A resolution: assignment of the carbonic anhydrase domain and evidence for structural heterogeneity within complex I. Biochim. Biophys. Acta 1777: 84–93. https://doi.org/10.1016/j.bbabio.2007.10.012

Pollastri, G., and A. McLysaght, 2005 Porter: a new, accurate server for protein secondary structure prediction. Bioinformatics 21: 1719–1720. https://doi.org/10.1093/bioinformatics/bti203

Pratje, E., C. Vahrenholz, S. Buhler, and G. Michaelis, 1989 Mitochondrial DNA of Chlamydomonas reinhardtii: the ND4 gene encoding a subunit of NADH dehydrogenase. Curr. Genet. 16: 61–64. https://doi.org/10.1007/BF00411086

Rackham, O., T. R. Mercer, and A. Filipovska, 2012 The human mitochondrial transcriptome and the RNA-binding proteins that regulate its expression. Wiley Interdiscip. Rev. RNA 3: 675–695. https://doi.org/10.1002/wrna.1128

Radermacher, M., T. Ruiz, T. Clason, S. Benjamin, U. Brandt *et al.*, 2006 The three-dimensional structure of complex I from Yarrowia lipolytica: a highly dynamic enzyme. J. Struct. Biol. 154: 269–279. https://doi.org/10.1016/j.jsb.2006.02.011

Radó-Trilla, N., and M. Albà, 2012 Dissecting the role of low-complexity regions in the evolution of vertebrate proteins. BMC Evol. Biol. 12: 155. https://doi.org/10.1186/1471-2148-12-155

Rahire, M., F. Laroche, L. Cerutti, and J. D. Rochaix, 2012 Identification of an OPR protein involved in the translation initiation of the PsaB subunit of photosystem I. Plant J. 72: 652–661. https://doi.org/10.1111/j.1365-313X.2012.05111.x

Remacle, C., D. Baurain, P. Cardol, and R. F. Matagne, 2001a Mutants of *Chlamydomonas reinhardtii* deficient in mitochondrial complex I: characterization of two mutations affecting the *nd1* coding sequence. Genetics 158: 1051–1060. https://www.ncbi.nlm.nih.gov/pmc/articles/PMC1461730/

Remacle, C., F. Duby, P. Cardol, and R. F. Matagne, 2001b Mutations inactivating mitochondrial genes in *Chlamydomonas reinhardtii*. Biochem. Soc. Trans. 29: 442–446. https://doi.org/10.1042/bst0290442

Remacle, C., G. Gloire, P. Cardol, and R. F. Matagne, 2004 Impact of a mutation in the mitochondrial LSU rRNA gene from *Chlamydomonas reinhardtii* on the activity and the assembly of respiratory-chain complexes. Curr. Genet. 45: 323–330. https://doi.org/10.1007/s00294-004-0490-z

Remacle, C., P. Cardol, N. Coosemans, M. Gaisne, and N. Bonnefoy, 2006 High-efficiency biolistic transformation of *Chlamydomonas* mitochondria can be used to insert mutations in complex I genes. Proc. Natl. Acad. Sci. USA 103: 4771–4776. https://doi.org/10.1073/pnas.0509501103

Remacle, C., M. R. Barbieri, P. Cardol, and P. P. Hamel, 2008 Eukaryotic complex I: functional diversity and experimental systems to unravel the assembly process. Mol. Genet. Genomics 280: 93–110. https://doi.org/10.1007/s00438-008-0350-5

Saada, A., R. O. Vogel, S. J. Hoefs, M. A. van den Brand, H. J. Wessels *et al.*, 2009 Mutations in *NDUFAF3* (*C3ORF60*),

encoding an NDUFAF4 (C6ORF66)-interacting complex I assembly protein, cause fatal neonatal mitochondrial disease. Am. J. Hum. Genet. 84: 718–727. https://doi.org/10.1016/j.ajhg.2009.04.020

Saint-Georges, Y., N. Bonnefoy, J. P. di Rago, S. Chiron, and G. Dujardin, 2002 A pathogenic cytochrome b mutation reveals new interactions between subunits of the mitochondrial bc1 complex. J. Biol. Chem. 277: 49397–49402. https://doi.org/10.1074/jbc.M207219200

Salinas, T., F. Duby, V. Larosa, N. Coosemans, N. Bonnefoy *et al*., 2012 Co-evolution of mitochondrial tRNA import and codon usage determines translational efficiency in the green alga Chlamydomonas. PLoS Genet. 8: e1002946. https://doi.org/10.1371/journal.pgen.1002946

Salinas, T., V. Larosa, P. Cardol, L. Marechal-Drouard, and C. Remacle, 2014 Respiratory-deficient mutants of the unicellular green alga Chlamydomonas: a review. Biochimie 100: 207–218. https://doi.org/10.1016/j.biochi.2013.10.006

Salinas-Giegé, T., M. Cavaiuolo, V. Cognat, E. Ubrig, C. Remacle *et al*., 2017 Polycytidylation of mitochondrial mRNAs in Chlamydomonas reinhardtii. Nucleic Acids Res. 45: 12963–12973. https://doi.org/10.1093/nar/gkx903

Sambrook, J., E. F. Fritsch, and T. Maniatis, 1989 *Molecular Cloning: A Laboratory Manual*. Cold Spring Harbor Laboratory Press, New York. 0879693096 9780879693091 0879693738 9780879693732

Sánchez-Caballero, L., B. Ruzzenente, L. Bianchi, Z. Assouline, G. Barcia *et al*., 2016 Mutations in complex I assembly factor TMEM126B result in muscle weakness and isolated complex I deficiency. Am. J. Hum. Genet. 99: 208–216. https://doi.org/10.1016/j.ajhg.2016.05.022

Schaefer, M. H., E. E. Wanker, and M. A. Andrade-Navarro, 2012 Evolution and function of CAG/polyglutamine repeats in protein-protein interaction networks. Nucleic Acids Res. 40: 4273–4287. https://doi.org/10.1093/nar/gks011

Schägger, H., and G. von Jagow, 1991 Blue native electrophoresis for isolation of membrane protein complexes in enzymatically active form. Anal. Biochem. 199: 223–231. https://doi.org/10.1016/0003-2697(91)90094-A

Schertl, P., S. Sunderhaus, J. Klodmann, G. E. Grozeff, C. G. Bartoli *et al*., 2012 L-galactono-1,4-lactone dehydrogenase (GLDH) forms part of three subcomplexes of mitochondrial complex I in Arabidopsis thaliana. J. Biol. Chem. 287: 14412–14419. https://doi.org/10.1074/jbc.M111.305144

Schimmeyer, J., R. Bock, and E. H. Meyer, 2016 L-Galactono-1,4-lactone dehydrogenase is an assembly factor of the membrane arm of mitochondrial complex I in Arabidopsis. Plant Mol. Biol. 90: 117–126. https://doi.org/10.1007/s11103-015-0400-4

Sen, S., D. Dash, S. Pasha, and S. K. Brahmachari, 2003 Role of histidine interruption in mitigating the pathological effects of long polyglutamine stretches in SCA1: a molecular approach. Protein Sci. 12: 953–962. https://doi.org/10.1110/ps.0224403

Sheftel, A. D., O. Stehling, A. J. Pierik, D. J. Netz, S. Kerscher *et al*., 2009 Human ind1, an iron-sulfur cluster assembly factor for respiratory complex I. Mol. Cell. Biol. 29: 6059–6073. https://doi.org/10.1128/MCB.00817-09

Shimogawara, K., S. Fujiwara, A. Grossman, and H. Usuda, 1998 High-efficiency transformation of *Chlamydomonas reinhardtii* by electroporation. Genetics 148: 1821–1828. https://www.genetics.org/content/148/4/1821

Silhavy, T. J., M. L. Berman, and L. W. Enquist, 1984 *Experiments with Gene Fusions*. Cold Spring Harbor Laboratory Press, Plainview, NY. ISBN: 0-87969-163-8

Subrahmanian, N., C. Remacle, and P. P. Hamel, 2016 Plant mitochondrial Complex I composition and assembly: a review. Biochim. Biophys. Acta 1857: 1001–1014. https://doi.org/10.1016/j.bbabio.2016.01.009

Subrahmanian, N., A. D. Castonguay, T. A. Fatnes, and P. P. Hamel, 2020 Chlamydomonas reinhardtii as a plant model system to study mitochondrial complex I dysfunction. Plant Direct 4: e00200. https://doi.org/10.1002/pld3.200

Tardif, M., A. Atteia, M. Specht, G. Cogne, N. Rolland *et al*., 2012 PredAlgo: a new subcellular localization prediction tool dedicated to green algae. Mol. Biol. Evol. 29: 3625–3639. https://doi.org/10.1093/molbev/mss178

van der Lee, R., M. Buljan, B. Lang, R. J. Weatheritt, G. W. Daughdrill *et al*., 2014 Classification of intrinsically disordered regions and proteins. Chem. Rev. 114: 6589–6631. https://doi.org/10.1021/cr400525m

Videira, A., and M. Duarte, 2002 From NADH to ubiquinone in Neurospora mitochondria. Biochim. Biophys. Acta 1555: 187–191. https://doi.org/10.1016/S0005-2728(02)00276-1

Vinothkumar, K. R., J. Zhu, and J. Hirst, 2014 Architecture of mammalian respiratory complex I. Nature 515: 80–84. https://doi.org/10.1038/nature13686

Viola, S., M. Cavaiuolo, D. Drapier, S. Eberhard, O. Vallon *et al*., 2019 MDA1, a nucleus-encoded factor involved in the stabilization and processing of the atpA transcript in the chloroplast of Chlamydomonas. Plant J. 98: 1033–1047. https://doi.org/10.1111/tpj.14300

Vogel, R. O., J. A. Smeitink, and L. G. Nijtmans, 2007 Human mitochondrial complex I assembly: a dynamic and versatile process. Biochim. Biophys. Acta 1767: 1215–1227. https://doi.org/10.1016/j.bbabio.2007.07.008

von Heijne, G., 1986 Mitochondrial targeting sequences may form amphiphilic helices. EMBO J. 5: 1335–1342. https://doi.org/10.1002/j.1460-2075.1986.tb04364.x

Watt, I. N., M. G. Montgomery, M. J. Runswick, A. G. Leslie, and J. E. Walker, 2010 Bioenergetic cost of making an adenosine triphosphate molecule in animal mitochondria. Proc. Natl. Acad. Sci. USA 107: 16823–16827. https://doi.org/10.1073/pnas.1011099107

Wostrikoff, K., Y. Choquet, F. A. Wollman, and J. Girard-Bascou, 2001 TCA1, a single nuclear-encoded translational activator specific for petA mRNA in Chlamydomonas reinhardtii chloroplast. Genetics 159: 119–132. https://www.ncbi.nlm.nih.gov/pmc/articles/PMC1461801/

Wydro, M. M., P. Sharma, J. M. Foster, K. Bych, E. H. Meyer *et al*., 2013 The evolutionarily conserved iron-sulfur protein INDH is required for complex I assembly and mitochondrial translation in Arabidopsis [corrected]. Plant Cell 25: 4014–4027 (erratum: Plant Cell 25: 4767). https://doi.org/10.1105/tpc.113.117283

Zhang, R., W. Patena, U. Armbruster, S. S. Gang, S. R. Blum *et al*., 2014 High-throughput genotyping of green algal mutants reveals random distribution of mutagenic insertion sites and endonucleolytic cleavage of transforming DNA. Plant Cell 26: 1398–1409. https://doi.org/10.1105/tpc.114.124099

Zhu, J., M. S. King, M. Yu, L. Klipcan, A. G. W. Leslie *et al*., 2015 Structure of subcomplex Iβ of mammalian respiratory complex I leads to new supernumerary subunit assignments. Proc. Natl. Acad. Sci. USA 112: 12087–12092. https://doi.org/10.1073/pnas.1510577112

Zickermann, V., S. Kerscher, K. Zwicker, M. A. Tocilescu, M. Radermacher *et al*., 2009 Architecture of complex I and its implications for electron transfer and proton pumping. Biochim. Biophys. Acta 1787: 574–583. https://doi.org/10.1016/j.bbabio.2009.01.012

Zickermann, V., C. Wirth, H. Nasiri, K. Siegmund, H. Schwalbe *et al*., 2015 Structural biology. Mechanistic insight from the crystal structure of mitochondrial complex I. Science 347: 44–49. https://doi.org/10.1126/science.1259859

Communicating editor: N. Louise Glass

Assembly of mitochondrial complex I requires the low-complexity protein AMC1 in *Chlamydomonas reinhardtii*

Nitya Subrahmanian[*†], Andrew David Castonguay[*‡], Claire Remacle[§], Patrice Paul Hamel[**].

*The Ohio State University, Department of Molecular Genetics, 500D Aronoff Laboratory, 318 W. 12th Avenue, Columbus, OH, 43210, USA.

† Plant Cellular and Molecular Biology Graduate Program, The Ohio State University, Columbus, Ohio, USA.

‡ Molecular Genetics Graduate Program, The Ohio State University, Columbus, Ohio, USA.

§University of Liège, Genetics and Physiology of Microalgae, UR InBios/Phytosystems, 4000 Liège, Belgium.

** The Ohio State University, Department of Molecular Genetics and Department of Biological Chemistry and Pharmacology, 500D Aronoff Laboratory, 318 W. 12th Avenue, Columbus, OH, 43210, USA.

SUPPORTING INFORMATION

Supporting Figures

Supporting Tables

Supporting Methods

SUPPORTING FIGURES

Figure S1. Sequence of the insertional *amc1-2* mutation in the *Cre16.g688900* gene of the *amc11* strain.

Black font depicts the section of exon 2 in the *Cre16.g688900* gene harboring the insertional *amc1-2* mutation in the *amc11* strain. **Orange bold font** indicates the insertional cassette conferring Hygromycin B resistance. The first 123 bp of the cassette, encoding the promoter region, was deleted upon insertion at this site. The **purple bold font** identifies the co-integrated herring sperm DNA sequences at the 5'- and 3'- ends of the cassette. The nucleotides with a black underline indicate the regions sequenced from TAIL-PCR or diagnostic PCR amplicons.

TGCATAGCTCCTGCCTTCTCACACAGTGGCTGGCGCGCAACGGCAGTAGCAACTG
GGACCTGTACCGGCTGCTACTGCGGCACCAGGCCGCGGCGGCGGCGGCGGCCG
CCGCAAGGCCCGATTTGGATACCATTGCAGTCGCGGTGCCGGGAACCGGCGGTC
AGGCTGGGATAAGTGACAATTTGAGAACATGTGCGGCGACGGCTGTGGCGAAAGC
GGTCTTGCAGCACAGCCGGAATGCAGCCCTCAAGCGCACCGGGCCCAACGGAAC
CGGTAGCGGTGACAGCGGATGGGTGGAGCCGCGGGCTGCGCTGCGACTGACGC
AGGCGCTGCGAGCGGCTCTGCCTTCCGCTACGGTTTCCCGCGGCAGCGGCGACG
CTTGGACCAGCCGCGGCGACGGCGCTGGTGCGGTGGTGGCGCCGGTGCCACGT
CAGGTGCGCGAGGCGGTGCGGGAGCTGCTGCTTGCTGCCGCCGCCCCCACCGG
GGCCCTCGGAGGCGGCAGCAGCGGTGCCGCAGGCGCTGCAGCAGGTGTTGGAG
CGGCGGGCGACGCAGTGGCGGCGGCCGGCCGGGAGGTGAGCTTCTGGATACGG
ACGGCGGCGGCCTTCACGTTGCCGCCGCACCCGGTCGGAGCGGCCGAGGCGGA
GTTGGTGGCGGGGCTGGGACCGGAGGCGGCGTTGGGTGGCGATCTGGCTGCGG
CCGCGGCGCCGCTGTTCCGCCGCGTCAGCCCGGACGCGCTGTTGGCCGCCGTCA
CCGACCTGGTACCTGGCGCGCAGCAACAGCAGCAACAGCAGCAACAGCAGCAAC
AGCAGCAACAGCAGCAACAGCAACAGCAGCAGCAGCAGGGCCCTGGCCT**AACAC**
GCACTGTAGCACACAAGTAAACGTTTGGCAAGCTTTTCAGGAATAGCGTGAACT
GAAAGAAAAAGAAGACTGCAAACCAGACGCCGACTCGGCCGTGTTGCTTTTGAA
ATTGAAAGTACCCTTGGGTGAACTTTGTCTTCGTGGTATTCTTGATTCTGATAGTC
TTTGTACAAATGTGTTTGCTCAACCATTTAGTTGTGAGCCCTGTAAAAAATGTTTT

CTCGACCGTTTTGTTGTGAGCCCTGTATGTTTCTAGCTTGCTTGCAACCATATAAA
CACCTTTGTTTCCATGGGTGTTTTGCTGTTCGTCTGTCCCCCAGATACAGACTGAA
TCTCCGAATCCAGGTTCTTGTTTATTTAGATTATTATGTTGGCCAAACCTCTTACA
CTGATTGTTCTGTTCAACCTAAAATAAAACAATTATAATCTAGGATATAAATTCTC
CCCGTCAACTATAAAAAAGGATGGATTTATGTTTATTGCAATACAAATACACCCTT
TTAAAAATGTATAACCTTGCCTACACTTTATGAACAACCCCTGTCTCCGTCCACCT
GCGACGTTGCATGGGCGCTCCGATGCCGCTCCAGGGCGAGCGCTGTTTAAATAG
CCAGGCCCCCGATTGCAAAGACATTATAGCGAGCTACCAAAGCCATATTCAAAC
ACCTAGATCACTACCACTTCTACACAGGCCACTCGAGCTTGTGATCGCACTCCGC
TAAGGGGGCGCCTCTTCCTCTTCGTTTCAGTCACAACCCGCAAACATGACACAAG
AATCCCTGTTACTTCTCGACCGTATTGATTCGGATGATTCCTACGCGAGCCTGCG
GAACGACCAGGAATTCTGGGAGGTGAGTCGACGAGCAAGCCCGGCGGATCAGG
CAGCGTGCTTGCAGATTTGACTTGCAACGCCCGCATTGTGTCGACGAAGGCTTTT
GGCTCCTCTGTCGCTGTCTCAAGCAGCATCTAACCCTGCGTCGCCGTTTCCATTT
GCAGCCGCTGGCCCGCCGAGCCCTGGAGGAGCTCGGGCTGCCGGTGCCGCCGG
TGCTGCGGGTGCCCGGCGAGAGCACCAACCCCGTACTGGTCGGCGAGCCCGGC
CCGGTGATCAAGCTGTTCGGCGAGCACTGGTGCGGTCCGGAGAGCCTCGCGTC
GGAGTCGGAGGCGTACGCGGTCCTGGCGGACGCCCCGGTGCCGGTGCCCCGCC
TCCTCGGCCGCGGCGAGCTGCGGCCCGGCACCGGAGCCTGGCCGTGGCCCTAC
CTGGTGATGAGCCGGATGACCGGCACCACCTGGCGGTCCGCGATGGACGGCAC
GACCGACCGGAACGCGCTGCTCGCCCTGGCCCGCGAACTCGGCCGGGTGCTCG
GCCGGCTGCACAGGGTGCCGCTGACCGGGAACACCGTGCTCACCCCCCATTCC
GAGGTCTTCCCGGAACTGCTGCGGGAACGCCGCGCGGCGACCGTCGAGGACCA
CCGCGGGTGGGGCTACCTCTCGCCCCGGCTGCTGGACCGCCTGGAGGACTGGC
TGCCGGACGTGGACACGCTGCTGGCCGGCCGCGAACCCCGGTTCGTCCACGGC
GACCTGCACGGGACCAACATCTTCGTGGACCTGGCCGCGACCGAGGTCACCGG
GATCGTCGACTTCACCGACGTCTATGCGGGAGACTCCCGCTACAGCCTGGTGCA
ACTGCATCTCAACGCCTTCCGGGGCGACCGCGAGATCCTGGCCGCGCTGCTCGA
CGGGGCGCAGTGGAAGCGGACCGAGGACTTCGCCCGCGAACTGCTCGCCTTCA
CCTTCCTGCACGACTTCGAGGTGTTCGAGGAGACCCCGCTGGATCTCTCCGGCTT
CACCGATCCGGAGGAACTGGCGCAGTTCCTCTGGGGGCCGCCGGACACCGCCC

CCGGCGCCTGATAAGGATCCCCGCTCCGTGTAAATGGAGGCGCTCGTTGATCTG
AGCCTTGCCCCCTGACGAACGGCGGTGGATGGAAGATACTGCTCTCAAGTGCTG
AAGCGGTAGCTTAGCTCCCCGTTTCGTGCTGATCAGTCTTTTTCAACACGTAAAA
AGCGGAGGAGTTTTGCAATTTTGTTGGTTGTAACGATCCTCCGTTGATTTTGGCCT
CTTTCTCCATGGGCGGGCTGGGCGTATTTGAAGCGGGTACCGGGCCCGTCATCC
CATGGAAGCTTCTTGCCGGGTGCACAGGCCTGTCACTTGTGCCTGTCTTAGTTGC
AGCAGTCGCCGGTGGACGGACCCTGGGCCTCGCCGGCCAGCACTGTGGACTGC
GCCGTGGGCGCCATGGATGCCCTGCTGCTGGACGCCGGCGCTGGCCAGCAACAC
CACCGGCAACAGCACCAACAGCACCCGCAACAGCACCAACAGCACCAAACTTCAC
ACCCGCAACAG

Figure S2. Sequence of the insertional *amc1-1* mutation in the *Cre16.g688900* gene of the *amc1* strain.

Black font depicts the section of exon 2 in the *Cre16.g688900* gene harboring the insertional *amc1-1* mutation in the *amc1* mutant. **Blue bold font** indicates the 1,536 bp of intergenic region from chromosome 17 inserted in exon 2. The **green bold font** and the **orange bold font** identify the co-integrated sequences at the 5'- and 3'- ends of the insertion site, respectively. The co-integrated sequence at the 5'-end (**green bold font**) has similarity to intron 24 of *Cre16.g695800*. The entire nucleotide sequence presented here was sequenced from TAIL-PCR and diagnostic PCR amplicons.

TGCATAGCTCCTGCCTTCTCACACAGTGGCTGGCGCGCAACGGCAGTAGCAACTG
GGACCTGTACCGGCTGCTACTGCGGCACCAGGCCGCGGCGGCGGCGGCGGCCG
CCGCAAGGCCCGATTTGGATACCATTGCAGTCGCGGTGCCGGGAACCGGCGGTC
AGGCTGGGATAAGTGACAATTTGAGAACATGTGCGGCGACGGCTGTGGCGAAAGC
GGTCTTGCAGCACAGCCGGAATGCAGCCCTCAAGCGCA**TAAACTCACTCTGACTC**
TCTCATGGCTGTCATCCGAGCCCCAGACTCTCCCCTCTCCCTATCTCTCCCCTAC
CCCACACCGCTGTGCCTGTTGCCCCCGACCTATCCCCGTAAGTCCTGAGCCGTTA
CCCGCAGCCCGTCAGTGATAGCCAAGGCCCCTGCCCACACTAGGGTCAAGAGTA
CCCCAACCCGCATAGCGTACGCCAGCAGAGCCTCTGCGCCAGGTTGCATACGTG
TAGTGTCTGGCAGCGATTAGGTACAGCAGCTGATAGCAGGGCGAGCTGGGAGC
GAGCCAGAGCAGGGTCCGGTTCGGTAGTTGGGCCTGAGCCCGTTCGGTTAGTGG
CAGTAGCAGGGAGTGAGGGAGACAGAGACGGGCGTAAGATAGCGTGAGATAGT
ACAGGGCCTGGGCCTAGGCAGTGGGGCGGACGGCATTGGACCGGGCACGCAC
GCCTTGTCTGCGGGTTGGGTCGTCGGGGGCTCTCCCCCCCCTTTCCCTTGGGGT
GTTCGCCTCCCCTGCCCCAGAGTGCAGGTCGACTGCGACACCTCTGGTCTGAAG
AAGTTTTGCTTATCCCTGCACCTGGTCTACCTGACCTGCGTGTGACCAAGTCCCC
GACACGCCGTGCCGGCTTGCGGGACCTGCTTGCTTTCCTGTCTCCCCTCTCTTCT
CCCTTCCCGTCTCTACCACCCGCCGCGTGCCCCGCACGCGAAGGGTAACCCCAG
CTACCGCCGGCGGCGGTGACTCTACTTGGGCAACCCGCCCGACCTTATCTCTCT
AATCTCTGATTACCCTGGGCGGCAAGGTTGAGTGAGACAGCCTTTGCCACGGCT
GTGCACCTGCACGCACGCCACCCATCCGGCTCTGTACGAGCCCCTGCTCCTGTT
ATCCAACCCGCCTAGACCAAACAGCGAAGCCCCTCCCGTGAGTAAAACAGCTAC

CGACGTCCCCATACGGCGGCGCTGGGCACTGCTGGGATCGAAGAGCCCCCTCT
ACGGCACGCGATCTGCCCCGACAGCTGTTGACACGCGGCGATAAAGTTAGGCG
AAAAAAGTGTCCTGTCATCTCTGGGGGGTCGGCACGCCTTTGTTGGTTTCGCTAC
CGGGACTTCTTCCATCCCCCAGTAGCCACTCATGTCAGACGAAGATGGCTTTCCC
CGCCGAGCGCGGCCTAGCGCTTTCCATACCGATCTGCAAGGACTTGACTATGAA
CGTATCACCCAACACTGCGAGCGCTTCGACCCGCAGTGGCATTCTGTGCGTGAT
TGACTGGAGTCCGTAGATGAGTTGGCAGAGGAATTCGGTTGGACTGAGTCACGA
AAGCTCCAACTTGCCTCTAAACGGCTTGGCCCCACGGCCAAGGAGTGGTACCGG
TCATGGAAGCTAGCCAACCCCATGGCATCGTCCACTTGGGAGGGCTTCTGTGAC
GCCCTGCGCGAGCGCTGGGGTGTGTCAGACCGCGAGCTGCATCTGGCCCTCGC
CAACTGCACACAAGGCCCCAAGGAGACGGTGCGCGAGTACGCCGACCGTTACC
TGGGCCTCGTGACCCAACTGCGCCTCGACTATAACCATCCGAGTGACCGGGCCC
AACGGAACCGGTAGCGGTGACAGCGGATGGGTGGAGCCGCGGGCTGCGCTGCG
ACTGACGCAGGCGCTGCGAGCGGCTCTGCCTTCCGCTACGGTTTCCCGCGGCAG
CGGCGACGCTTGGACCAGCCGCGGCGACGGCGCTGGTGCGGTGGTGGCGCCGG
TGCCACGTCAGGTGCGCGAGGCGGTGCGGGAGCTGCTGCTTGCTGCCGCCGCCC
CCACCGGGGCCCTCGGAGGCGGCAGCAGCGGTGCCGCAGGCGCTGCAGCAGGT
GTTGGAGCGGCGGGCGACGCAGTGGCGGCGGCCGGCCGGGAGGTGAGCTTCTG
GATACGGACGGCGGCGGCCTTCACGTTGCCGCCGCACCCGGTCGGAGCGGCCG
AGGCGGAGTTGGTGGCGGGGCTGGGACCGGAGGCGGCGTTGGGTGGCGATCTG
GCTGCGGCCGCGGCGCCGCTGTTCCGCCGCGTCAGCCCGGACGCGCTGTTGGC
CGCCGTCACCGACCTGGTACCTGGCGCGCAGCAACAGCAGCAACAGCAGCAACA
GCAGCAACAGCAGCAACAGCAGCAACAGCAACAGCAGCAGCAGCAGGGCCCTGG
CCTGGGTGAGCAACCGCGTGCCAGGAAGGGACCCTCGCTGTCAT

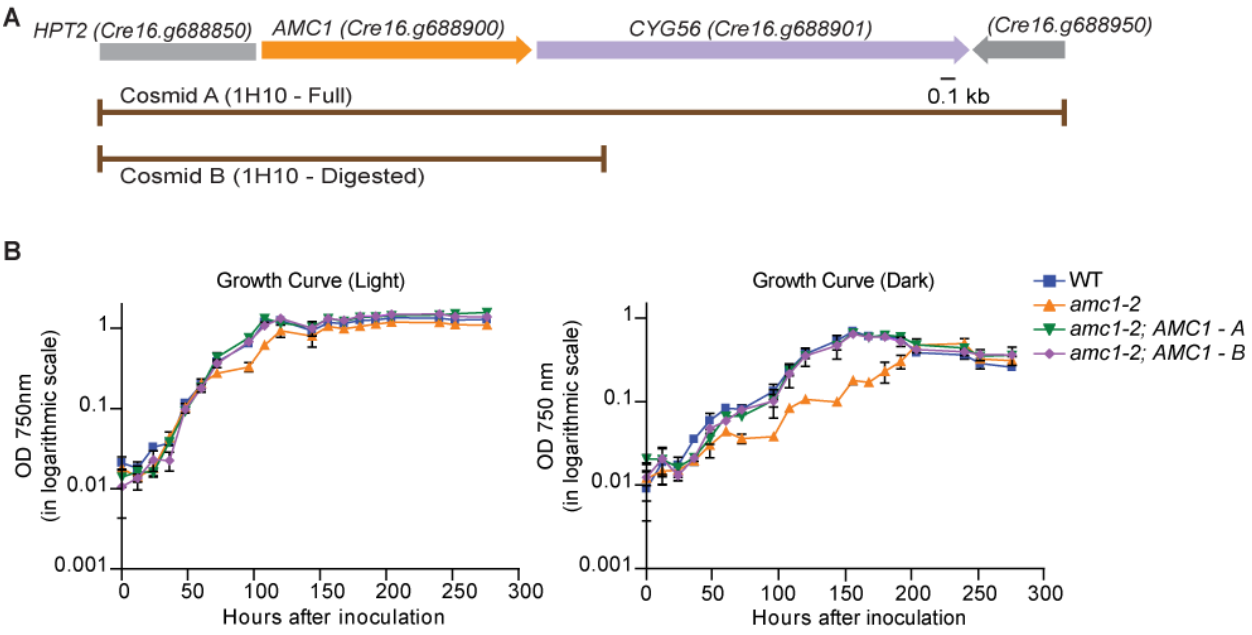

Figure S3. Rescue of the SID phenotype with cosmids containing the wild-type *AMC1* genomic DNA.

(A) Simplified map of the *Chlamydomonas* genomic DNA contained in the cosmids used for complementation studies. The 1H10 (Cosmid A) carries the truncated *HPT2* gene (*Cre16.g688850*), the *AMC1* gene (*Cre16.g688900*), the *CYG56* gene (*Cre16.g688901*), and *Cre16.g688950*. Cosmid 1H10 was digested by *Bam*HI restriction enzyme to obtain a truncated cosmid (Cosmid B) that only retains one full-length gene, namely *AMC1*. Both cosmids were used to transform the *amc1-2* mutant strain *amc11 (10G11)*.

(B) The growth of WT, *amc1-2* [*amc11 (10G11)*], [*amc1-2; AMC1-A*], and [*amc1-2; AMC1-B*] was documented by measuring optical density at A_{750}, in the light or in the dark, in the presence of acetate as a carbon source. The average of three biological replicates is reported here, with error bars indicating standard deviation of the mean. The generation time calculated from these growth curves is displayed in Figure 3A.

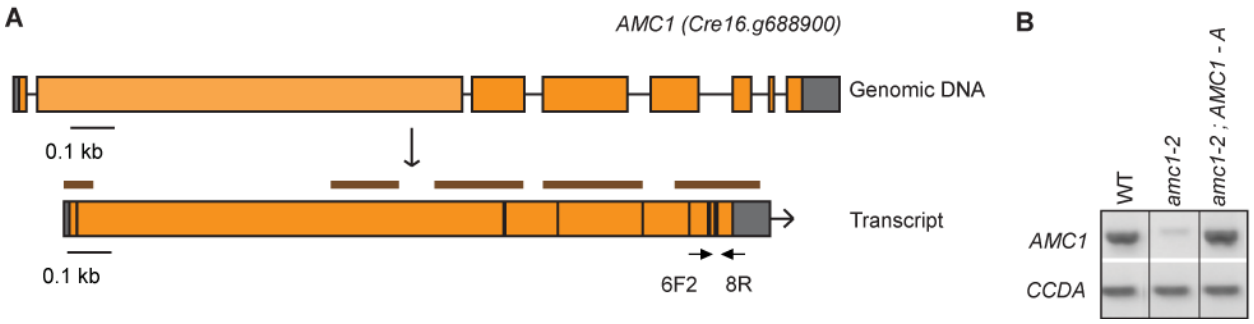

Figure S4. Transcript levels in the *amc1-2* mutant are restored by *AMC1* genomic DNA.

(A) The current *Chlamydomonas* genome database JGI v5.5 predicts the model for the *AMC1* gene as represented in the top panel. This gene model was experimentally corroborated by PCR amplification using *AMC1*-specific primers with total cellular cDNA prepared from the wild-type (4C$^-$). The brown lines, in the bottom panel, identify the sections of the *AMC1* cDNA successfully amplified and confirmed by sequencing. The following primer pairs were successful in amplifying the sequence of the *AMC1* cDNA: Cre16.g688900 5′UTR-F1/E2R10; 10G11 exon2F (1) / amc11-del1R; Cre16.g688900 exon2F4/exon3R2; au5.g6830 exon3F / exon4R; Cre16.g688900 exon4F2 / exon4-3R; Cre16.g688900 exon5-F3 / exon-8R; Cre16.g688900 exon8-1F / Cre16.g688900 3′UTR-1R; Cre16.g688900 exon8-1F / 3′UTR-2R (Table S2).

(B) Transcript abundance of *AMC1* was analyzed by RT-PCR in the wild-type (4C$^-$), *amc1-2* [*amc11 (10G11)*] strain, and the complemented strain [*amc1-2; AMC1-A*]. The *AMC1*-specific primers (au5.g6830 6F2 / Cre16.g688900 8R), used for amplification, are represented in (Figure S4A) with black arrows. *CCDA,* a gene involved in photosynthesis (GABILLY *et al.* 2011), was used as control for constitutive expression. Three independent biological replicates were performed, and one representative is shown in this figure. The vertical black lines indicate assembly of different lanes from the same gel.

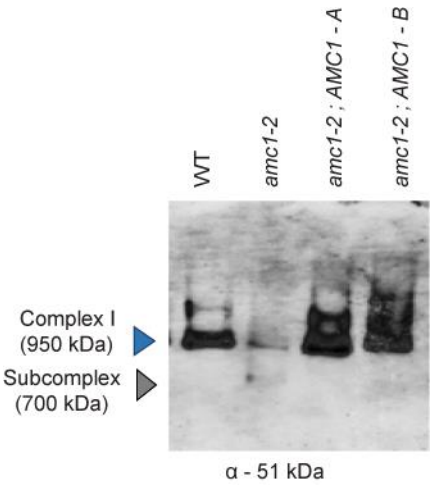

Figure S5. The *amc1-2* mutant display traces of a fully-assembled complex.
Immunoblotting using anti-51 kDa antibody of complexes separated by BN-PAGE. Two hundred µg of protein were loaded per lane. While the labile 700 kDa subcomplex can always be detected in the *amc1-2* mutant, in occasional membrane extractions, low levels of a fully-assembled complex I were also detected.

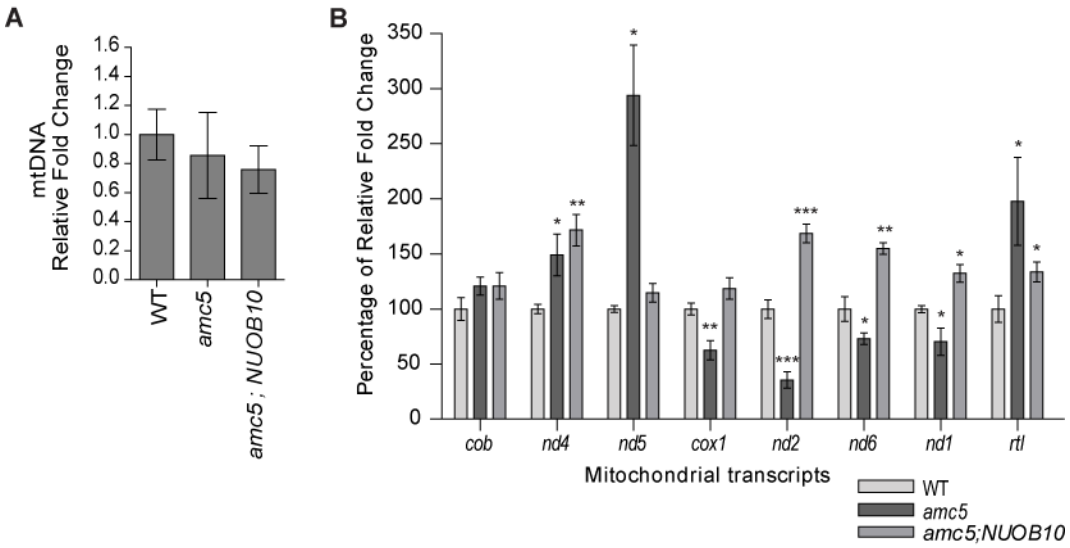

Figure S6. Mitochondrial transcript levels in a nuclear mutant characterized by the loss of the complex I subunit NUOB10.

(A) Real-time quantitative PCR (qPCR) was used to assess the relative quantity of mtDNA. The mitochondrial *nd4* gene was used as a target gene and the nuclear gene *TUA2,* encoding the alpha tubulin 2 protein, was used as the reference gene. The average was obtained from two biological replicates, each including three technical replicates, and the error bars represent standard deviation of the mean. The results are represented as fold change relative to WT (WT set to 1.0).

(B) Real-time quantitative PCR (qPCR) was used to assess the relative abundance of the mitochondrial transcripts, *cob, nd4, nd5, cox1, nd2, nd6, nd1*, and *rtl.* The strains tested were WT ($3A^+$), *amc5 (87D3)*, *and* [*amc5; NUOB10*]. The relative abundance of the mitochondrial transcripts was determined with respect to the geometric mean of the three reference transcripts *CBLP, TUA2*, and *EIFA.* The average is represented from three biological replicates, each analyzed in two technical replicates. The error bars represent standard deviation of the mean. The results are represented as percentage of fold change relative to WT (WT set to 100). The significance of difference in transcript abundance was determined with respect to the corresponding WT by two-tailed unequal variances *t*-test. The symbol * represents $p<0.05$, ** represents $p<0.01$, and *** represents $p<0.001$.

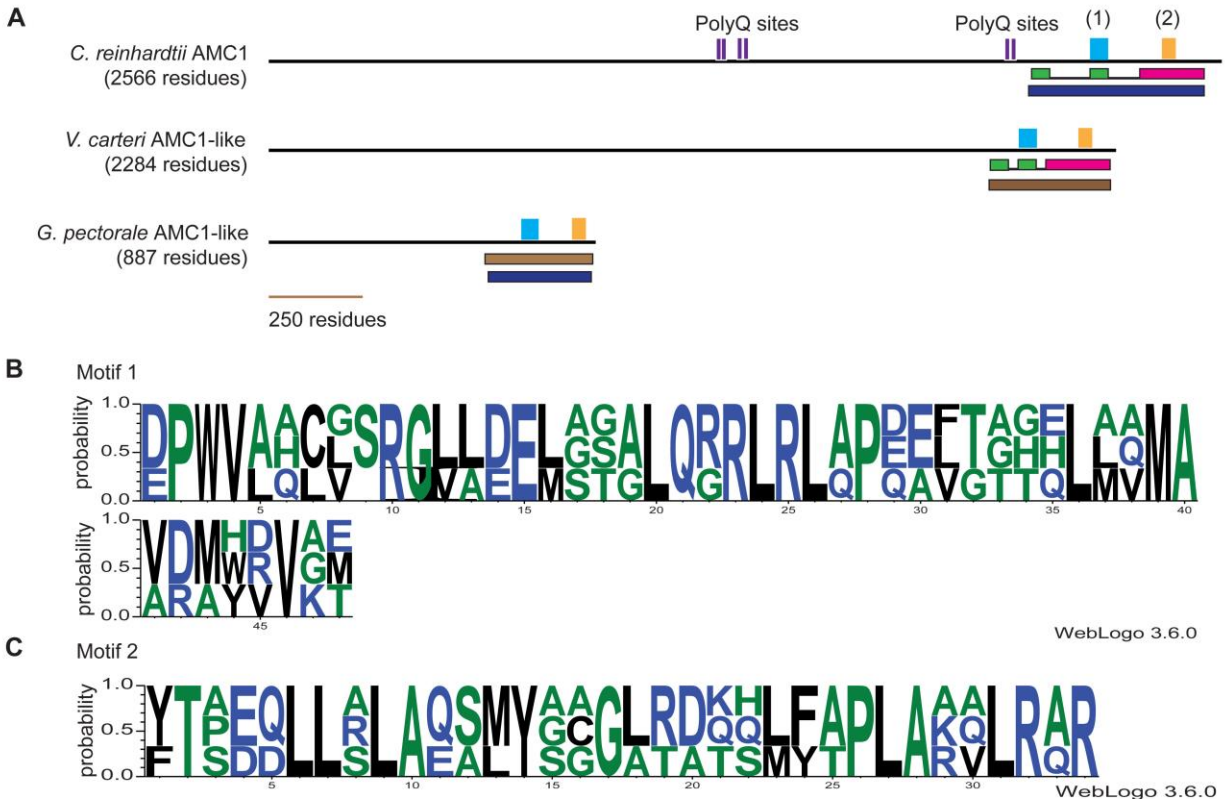

Figure S7. The C-terminus of AMC1 is similar to that of hypothetical algal proteins in *Volvox carteri* and *Gonium pectoral.*

Searches for AMC1-like proteins, via BLASTp (ALTSCHUL *et al.* 1990) and DELTA-BLAST (BORATYN *et al.* 2012), revealed that the AMC1 C-terminus (202 residues) has 37% identity with the C-terminus of another large hypothetical protein (2284 aa) from a closely related chlorophycean green alga *Volvox carteri* (Phytozome 12 Volvox database v2.1 ID: Vocar.0023s0109.1 / NCBI Accession: XP_002952084.1). AMC1 and the hypothetical *Volvox* protein show similarity at the C-terminus with another putative protein (887 aa in length) from the green alga *Gonium pectorale* (GPECTOR_23g121 / NCBI accession KXZ49034). While AMC1 shows only a weak similarity (29% identity amongst 432 residues), the *Volvox* hypothetical protein shows a significant similarity (36% identity amongst 339 residues) with the C-terminal region of the *Gonium* hypothetical protein.

(A) Conserved C-terminal motifs and polyQ repeats in the AMC1 protein sequence are shown. The polyQ repeats shown in Figure 7 are represented here as purple bars. Similarity searches with AMC1 identified similarity in the C-terminal end within a *Volvox*

carteri hypothetical protein. The pink box depicts 46% similarity in a 202 amino acid region, whereas the green boxes depict 64-68% in a 45 amino acid region. Subsequent similarity searches using the *Volvox* AMC1-like protein yielded a *Gonium pectorale* hypothetical protein. The brown box depicts a 296 amino acid region with 46% similarity to *Gonium* hypothetical protein. The dark blue box depicts the region of low similarity (36%) between the *Chlamydomonas* AMC1 protein and the *Gonium* hypothetical protein. Comparison of these three proteins using the MEME program (BAILEY *et al.* 2009) identified the presence of two different motifs (motif 1 and motif 2, represented by a light blue box and a yellow box, respectively) that is common to the C-terminus of all three proteins. The sequence of these motifs in AMC1 are represented in Figure 7b.

(B) and **(C)** are the MEME-generated consensus sequences for motif 1 and motif 2, respectively (BAILEY *et al.* 2009). Motifs 1 and 2 are predicted to be 48 and 34 residues in length, respectively. The height of each letter represents the frequency of occurrence of the corresponding amino acid (y-axis) at a given position in the motif (x-axis). The *E-value* for the occurrence of motif 1 and motif 2 are $1.3e^{-006}$ and $1.8e^{-004}$, respectively.

SUPPORTING TABLES

Table S1. List of reference numbers for key *Chlamydomonas* strains used in this study.

Strain name	Genotype	Chlamydomonas collection center reference number
3A^{+}	*mt*$^{+}$; *arg7-8*	CC-5589
4C^{-}	*mt*$^{-}$; *arg7-8*	CC-5590
amc5 (87D3)	*mt*$^{+}$; *arg7-8*; *nuob10::APHVIII*	CC-5591
amc5; NUOB10	*mt*$^{+}$; *arg7-8*; *nuob10::APHVIII; NUOB10; ARG7*	CC-5592
amc1 (4C10)	*mt*$^{+}$; *arg7-8*; *amc1-1*; *APHVII*	CC-5597
amc1(2)	*mt*$^{+}$; *amc1-1*	CC-5598
amc1(27)	*mt*$^{-}$; *arg7-8; amc1-1*	CC-5599
amc11 (10G11)	*mt*$^{-}$; *arg7-8*; *amc1-2; APHVII*	CC-5608
amc1-2; AMC1-A	*mt*$^{-}$; *arg7-8*; *amc1-2; APHVII; AMC1; ARG7*	CC-5609
amc1-2; AMC1-B	*mt*$^{-}$; *arg7-8*; *amc1-2; APHVII; AMC1; ARG7*	CC-5610
amc11(65)	*mt*$^{-}$; *amc1-2; APHVII*	CC-5614

Table S1. List of reference numbers for key *Chlamydomonas* strains used in this study.

A list of the main strains used in this study is provided here with their genotypes and the reference number for retrieval from the *Chlamydomonas collection center* (chlamycollection.org).

Table S2. Sequence of primers.

Primer Name	Sequence (5' to 3')	Target
Cre16.g688900 5'UTR F1	GCACAGCCACACATGCATAAC	*AMC1* *(Cre16.g688900)*
10G11 exon2F (1)	GGTCAGGCTGGGATAAGTG	
10G11 AD1-F (2)	TACTGTTGCGGGTGCTG	
au5.g6830 exon2F2	TGCATAGCTCCTGCCTTCTC	
au5.g6830 exon2F3	AGGTGAGCTTCTGGATACG	
Cre16.g688900 exon2F4	CTGCGGAAAGGTGGCTTGAC	
Cre16.g688900 E2F32	TGGCGGGTGCCGCGCTGTTC	
Cre16.g688900 E2F33	CGCTGGTGCTGACGATAATG	
amc11 del1R	ATGACAGCGAGGGTCCCTTC	
Cre16.g688900 E2R9	GTGCTGCAAGACCGCTTTC	
Cre16.g688900 E2R10	TGTAGGACCGCCGGAGGCTTG	
au5.g6830 exon 3F	GCTACGGATGGCGAGGTG	
Cre16.g688900 exon3R2	GACGTGGCTTCCAGCTGTTG	
Cre16.g688900 exon4 F2	GGACACGTTGCAGAGGCAACAG	
au5.g6830 exon 4R	GTGCTGCGGAGTGTTATCG	
Cre16.g688900 exon4-3R	CAGGCACGCGGCCACCCCACGG	
Cre16.g688900 exon5 F3	CCAGCACCAGCATTCCATAG	
au5.g6830 exon6F2	CTGAGGGACACCAGTCTGTTC	
Cre16.g688900 exon8-1F	CTGTGAGCGGGATGAAAGG	
Cre16.g688900 exon8 R	AGGTGACTCGGCACCAAC	
Cre16.g688900 3'UTR-1R	AAGAGGTCACTGCCGTTCAC	
Cre16.g688900 3'UTR-2R	CCCGCATTGATGAACTTG	
PHA-F	CACACACGAATTCGATATCAAGCTGGAAGCTTAT GCGCGAGCATGCTGTGC.	

PHA-R	AAATACCGGCGATTTTTCGGCATTCATAAGCTTA ACCCCCTCGGGTGGCAGC.	
AD1	NTCASTWTSGWGTT	Partially degenerate primers used for TAIL-PCR
AD2	NGTCGASWGANAWGAA	
RMD228	WGNTCWGNCANGCG	
APH7R5	CGGTCGAGAAGTAACAGGG	iHyg3
APH7F3	CGACGTCTATGCGGGAGACT	
APH7F5	AACTGCATCTCAACGCCTTCC	
APH7F8	ACTGCTCGCCTTCACCTTC	
amc1-insert-R2	GGTACTCTTGACCCTAGTG	*amc1* insertion
amc1 insert F1	AGATAGCGTGAGATAGTACAG	
ND5-EG-F2	GATACCCTCCCAACCAACAAGCATAAC	*nd5*
cox1-R	CCGAATAGGGCTGGCATTAC	*cox1*
CCDA.13	GCCACATTCGCACTGGC	*CCDA*
CCDA.14	GGAGTCACCCAGGCCGAGTAC	

Table S2. Sequence of primers.

List of primers used for TAIL-PCRs, diagnostic PCRs, and RT-PCRs.

Table S3. Primers used for qRT-PCR.

Primer name	Sequence (5' to 3')	Target	Amplicon	Efficiency (%)	r^2 value
Chlamy cob fw	GCCTACCCAACTCCAATGAA	*cob*	192 bp	98.0	0.999
Chlamy cob rev	GTGAGCGTAACGCAAGATCA				
Chlamy nd4 fw	ACACTATGGCCGGTTCTTTG	*nd4*	213 bp	98.0	0.998
Chlamy nd4 rev	CACTACCAGCAGTTGGAGCA				
Chlamy nd5 fw	CCCCAATTGCTCGTTTTCTA	*nd5*	226 bp	97.0	0.997
Chlamy nd5 rev	CCGGTAACGGTGAATAGCAT				
Chlamy cox1 fw	TGGTAATGCCAGCCCTATTC	*cox1*	181 bp	98.0	0.999
Chlamy cox1 rev	TAAGCGGTCCAACCAGTACC				
Chlamy nd2 fw	CCACCATTTGCAGGTTTCTT	*nd2*	210 bp	100.0	0.999
Chlamy nd2 rev	GCAGGCAGAGGTTAGAGTGG				
Chlamy nd6 fw	TATTTTGTTGTGCGCTTTGC	*nd6*	220 bp	99.0	0.999
Chlamy nd6 rev	TAGCTCAGTGGCTGGGATCT				
ND1F2	GATCTACCAGAGGCTGAGTTG	*nd1*	150 bp	102.0	0.94
ND1R1	TTTAAGGGCGCTGAAGCCAC				
Chlamy rtl fw	CTGCCCTGCTTCTAATGGAG	*rtl*	231 bp	103.0	0.998
Chlamy rtl rev	TACCAAAACCAGGACGGAAG				

Cre16.g688900 exon5-1F	GGCCTGGCCGAGGAGATGGG	*AMC1*	82 bp	96.8	0.974
Cre16.g688900 exon5-2R	AGCAACTGGTGGGCTGTGAG				
EIFA FW	CATTGTGGAGCCGCCATTTC	*EIFA*	122 bp	99.8	0.997
EIFA REV	GGCTGCTTGCATTTGCTTCC				
CBLP-F	GCCACACCGAGTGGGTGTCGTGCG	*CBLP*	201 bp	108.0	0.9961
CBLP-R	CCTTGCCGCCCGAGGCGCACAGCG				
Tub-F	GTCCAAGCTGGGCTTCACCGTC	*TUA2*	152 bp	104.0	0.9908
Tub-R	GGCGGCAGATGTCGTAGATGGC				

Table S3. Primers used for qRT-PCR.

The sequences of primers used for qRT-PCR, with the resultant amplicon size, are shown here. The amplification efficiency for gene-specific primers, for the mitochondrial targets *cox1*, *nd4*, *nd5*, *cox1*, *nd2*, *nd6*, *nd1*, *rtl* (WOBBE AND NIXON 2013), and nuclear targets *CBLP* (ALLEN *et al.* 2007), *TUA2* (VALLEDOR *et al.* 2013), and *EIF1A* (SCHMOLLINGER *et al.* 2014) was identified by generating calibration curves with cDNA dilutions. The r^2 value for PCR efficiency, calculated from each calibration curve, are reported here. These PCR efficiencies were used in calculating the relative expression ratio by the Livak Method (LIVAK AND SCHMITTGEN 2001). The Phytozome IDs of nuclear genes are: *TUA2* - Cre04.g216850, *CBLP* - Cre13.g599400, *EIF1A* -Cre02.g103550.

SUPPORTING MATERIALS AND METHODS

Method S1. Genetic analysis

Genetic crosses were conducted according to (HARRIS 1989). Gametogenesis was induced by resuspending vegetative cells in TAP liquid medium lacking nitrogen (TAP-N), at 25° in low light (0.5-1.0 µmol. m^{-2}. s^{-1}), with shaking for 5 h. The gametes were mixed in equal proportions and incubated in light (50 µmol. m^{-2}. s^{-1}) at 25° overnight. To isolate meiotic zygotes, the mixture was plated on TAP-N solid medium (containing 3% (w/v) select agar) and incubated in light (50 µmol. m^{-2}. s^{-1}) at 25° for 5 days. The meiotic progeny was obtained through bulk germination on TARG solid medium, in continuous light at 25°. To isolate vegetative diploids, the mating mixture was directly plated on selective medium mentioned below. Individual diploids and haploid progeny were sub-cloned to a single colony on solid medium and their mating type was determined by diagnostic PCR (WERNER AND MERGENHAGEN 1998).

To determine the segregation of the SID phenotype in the *amc11* mutant, wild-type strain 1' (*mt*$^+$) [a *137C* derivative, kindly provided by Dr. Claire Remacle, University of Liège, Belgium] was mated with *amc11 (10G11)* (*mt*$^-$; *amc1-2*; *APHVII; arg7-8*). After bulk germination of the meiotic zygotes, haploid progeny were plated on TARG medium and the relevant phenotypes of the progeny were deduced by replica-plating. The haploid progeny derived from these crosses, *amc11 (65)* (*mt*$^-$; *amc1-2; APHVII),* was retained for further analyses.

To test whether the *amc1* and *amc11* mutations are allelic, *amc11 x amc1* diploids were generated by crossing *amc1(2) (mt*$^+$; *amc1-1)* with *amc11 (10G11)* (*mt*$^-$; *amc1-2*; *APHVII; arg7-8*) with selection on TAP + HyB solid medium. In addition, haploid progeny from the *amc11 x amc1* cross were obtained by crossing *amc1(2) (mt*$^+$; *amc1-1)* with *amc11(65) (mt*$^-$; *amc1-2; APHVII).* The meiotic zygotes were bulk-germinated and the haploid progeny (98 colonies) was tested for the relevant growth phenotypes by replica-plating.

Method S2. Genomic DNA extraction and diagnostic PCR

Genomic DNA was extracted from *Chlamydomonas* by phenol-chloroform method (SAMBROOK *et al.* 1989). The sequences of primers used in diagnostic PCRs and TAIL-

PCRs are provided in Table S2. For diagnostic PCR analysis, GoTaq Polymerase (Promega, M3008) was used according to manufacturer's protocol, with the addition of 2.5% (v/v) DMSO. Note that a denaturation temperature of 98º was used for *Chlamydomonas* genomic DNA / cDNA templates. The primers used for generating the amplicons in Figure 1D and the corresponding amplicon sizes are as follows: A [Cre16.g688900 E2F33 / E2R9, 400 bp]; B [10G11 exon2F (1) / 10G11 AD1-F (2), 881 bp]; C [au5.g6830 exon2F3 / 10G11 AD1-F (2), 469 bp]; D [10G11 exon2F (1) / amc1-insert-R2, 280 bp]; E [APH7F8 / 10G11 AD1-F (2), 592bp].

Method S3. TAIL-PCR (Thermal Asymmetric Interlaced PCR)

TAIL-PCR was used to identify the sequence flanking the insertional cassette in the *amc11 (10G11)* mutant as in (LIU *et al.* 1995). The following partially degenerate primers were used for TAIL-PCR: AD1, AD2, and RMD228 (LIU *et al.* 1995; DENT *et al.* 2005). The iHyg3-specific primers, APH7F3, APH7F5, and APH7F8, were used to amplify the genomic DNA flanking the cassette at its 3′-end. The site of insertion was identified as exon 2 of gene *Cre16.g688900*, as provided by the *Chlamydomonas* genome database version 5.5 in Phytozome version 12 (https://phytozome.jgi.doe.gov/pz/portal.html#!info?alias=Org_Creinhardtii) (BLABY *et al.* 2014). The sequence flanking the 5′-end of the cassette was obtained by conventional PCR, using the *AMC1*-specific primer au5.g6830 exon2F3 and the iHyg3-specific primer APH7R5 (Figure S1).

To identify the *amc1* mutation, diagnostic PCR was conducted and an insertional mutation was identified in exon 2. TAIL-PCR was used to identify the insertional sequence disrupting the *AMC1* gene in the *amc1-1* mutant by analyzing two independent *amc1-1* strains: *amc1 (4C10)* and *amc1 (27).* Two sets of TAIL-PCR reactions were successful. In both, the partially degenerate primer RMD228 was used, in combination with the following *AMC1*-specific primers (for primary, secondary, and tertiary reactions, respectively): A) Cre16.g688900 E2F32, Cre16.g688900 E2F33, and au5.g6830 exon2F2, and B) Cre16.g688900 E2F33, au5.g6830 exon2F2, and 10G11 exon2F (1). The complete sequence was retrieved by amplification with the primer pair amc1insertF1/amc11del-R. The inserted DNA, disrupting the *AMC1* gene, was confirmed

by sequencing two independent *amc1-1* strains: the original *amc1 (4C10)* and its haploid progeny *amc1(27)* (Figure S2).

Method S4. PCR-based screening of *Chlamydomonas* genomic library

An *ARG7*-based indexed cosmid library of *Chlamydomonas* genomic DNA, created by Dr. Jean David Rochaix's laboratory (University of Geneva, Switzerland) (PURTON AND ROCHAIX 1994), was screened for the presence of cosmids carrying the *AMC1* gene by diagnostic PCR. The *AMC1*-containing cosmid (referred to as 1H10) was identified using the primer pair au5.g6830 exon2F3/10G11 AD1-F (2). In order to generate a construct containing only the full-length *AMC1* gene, the cosmid 1H10 was digested with *Bam*H1 restriction enzyme and recircularized by T4 DNA ligase (Invitrogen, 15224041). The borders of *Chlamydomonas* genomic DNA insert, present in the original cosmid 1H10 (referred to as cosmid A) and the *Bam*HI digested and re-ligated cosmid (referred to as cosmid B) were sequenced to confirm the presence of the region carrying the gene of interest (Figure S3A).

Method S5. Biolistic transformation

Cosmids A and B were used for transformation by biolistics. The *ARG7* gene in the cosmids was used as a selection marker. The recipient arginine auxotrophic strain *amc11 (10G11) (mt*$^-$; *amc1-2*; *APHVII*; *arg7-8)*, also referred to as the *amc1-2* mutant in this manuscript, was subjected to biolistic transformation using a homemade particle delivery device. The strains were grown in liquid TARG medium for 2-3 days until they reached exponential phase (3 – 6 x 10^6 cells. mL^{-1}). The cells were plated on selective TAP medium at 10^8 cells/plate. For each bombardment, DNA was coated on sterile 0.6-0.9 µm tungsten particles (STREM Chemicals, 93-7437) by using 2 µg of cosmid, 16.7 mM Spermidine (Sigma, S2626-5G), and 1 M $CaCl_2$. The bombardment was conducted at a helium pressure of 1.725 MPa and vacuum of -92 kPa. The plate was positioned 10.5 cm away from the nozzle containing the coated particles. The bombarded plates were first incubated at low light overnight for recovery and then transferred to continuous light (50 µmol. m^2. s^{-1}).

Transformants from cosmid A were screened by replica-plating. Out of 311 transformants tested, 115 transformants displayed rescued growth in the dark. Transformants from

cosmid B were screened by serial dilution. Out of 45 transformants, at least 40 displayed restoration of growth in the dark. Two transformants (two each for cosmids A and B), displaying rescued growth in the dark, were tested for biochemical activity and confirmed for complex I activity restoration. Out of the two, one transformant with cosmid A and one transformant with cosmid B were retained for further analysis.

Method S6. RNA extraction, RT-PCR, and qPCR

To determine the *AMC1* gene model (Figure S4), RNA was prepared using the Plant RNeasy Kit (Qiagen, 74904) with the following modifications. Cells were grown for 2-3 days on TARG solid medium. Cells (100 mg) were harvested and lysed by vortexing, with 9/10th volume of glass beads, for 5 min at 22º. RNA extraction was completed according to manufacturer's protocols. WT (4C^{-}) RNA (2-5 µg) was treated with RQ1 RNase-free DNase I (Promega, M6101). Reverse-transcription was achieved with 400 units of M-MLV reverse transcriptase (Life Technologies, 28025-013). Some regions of the cDNA could be amplified only if the first strand synthesis was conducted with Roche Transcriptor High Fidelity cDNA synthesis kit (05081955001), using OligodT primers or random hexamers as per manufacturer's protocol. Different regions of the *AMC1* cDNA were successfully amplified using either GoTaq Polymerase (Promega, M3008) or Phusion High-Fidelity DNA Polymerase (NEB, B0519S). The primer pairs used for successfully sequenced cDNA amplicons are provided in the legend of Figure S4. The amplicon generated using Cre16.g688900 5′UTR-F1/E2R10 was cloned into Promega pGEM-T easy Vector System. The resulting construct contains the sequence corresponding to the AMC1 N-terminal that was cloned in-frame to the *ubiG* reporter.

For real-time quantitative PCR (qPCR) of the mitochondrial transcripts, RNA was isolated by phenol-chloroform method modified from (NEWMAN *et al.* 1990). RNA was extracted from 2 x 10^{8} cells grown in liquid culture. The cells were first resuspended in TEN buffer (10 mM Tris-HCl pH 8.0, 10 mM EDTA, 150 mM NaCl) and pelleted. The cells were resuspended in 150 µl of water and 300 µl of SDS-EB buffer (2% SDS, 400 mM NaCl, 40 mM EDTA, 100 mM Tris-HCl pH 8.0). Nucleic acids were extracted twice with equal volume of phenol-chloroform (pH 5.0) and RNA was precipitated with 1/3rd volume of 8 M LiCl. RNA (8 µg) was treated with RQ1 RNase-free DNase I (Promega, M6101). Reverse

transcription was achieved with 800 units of M-MLV Reverse transcriptase (Life Technologies, 28025-013) using 1 µg of Random Hexamers (Promega, C1181), according to the manufacturer's protocol. The absence of contaminating mtDNA was confirmed by diagnostic PCR of cDNA sample, across the two transcription start sites, with the primer pair ND5-EG-F2 and cox1-R (Table S2). The qPCR was conducted simultaneously on two dilutions of the cDNA and the results were compared for correlation. Amount of cDNA equivalent to 50 ng or 100 ng of total input RNA was used as template for qPCR using SensiMix (Bioline, QT-650-05) on a Mastercycler ep gradientS realplex thermocycler (Eppendorf). The qPCR reactions were denatured at 98º for 15 s, annealed at 60º for 20 s and extended at 72º for 20 s. Relative transcript levels were determined by normalizing the levels of target transcripts to the geometric mean of three reference transcripts, *TUA2, CBLP*, and *EIF1A.* For determining the relative mitochondrial DNA (mtDNA) content, 8 ng of total genomic DNA was used as template for qPCR. The mitochondrial *nd4* gene was used as the target gene and the nuclear *TUA2* gene was used as the reference. In all cases, normalization of target transcript or gene levels to the reference was performed by the Livak $2^{-\Delta\Delta Ct}$ method (LIVAK AND SCHMITTGEN 2001). Relative fold change for mtDNA content was calculated by normalizing to the average of the isogenic wild-type strain (set to 1.0). Relative transcript abundance is represented as percentage of wild-type strain. The amplification efficiency for each primer pair was determined by generating calibration curves for each pair of primers using two-fold dilutions of the template (wild-type cDNA). The efficiency was calculated from the slope of the calibration line as $[10^{(-1/slope)}-1] \times 100$. The efficiency and r^2 value from the calibration line are reported in Table S3. In Figure 6C, the *amc1-1* and *amc1-2* mtDNA content were normalized to their respective WT, $3A^+$ and $4C^-$, respectively. The strains tested in Figure 6D are WT ($4C^-$), *amc1-2* [*amc11 (10G11*)], and [*amc1-2; AMC1-B*]. The strains tested in Figure 6E are WT ($3A^+$) and *amc1-1* [*amc1(4C10*)].

Method S7. Plasmid construction to test for mitochondrial localization

The AMC1 N-terminal mitochondrial targeting sequence was heterologously expressed as a translational fusion with the bacterial UbiG protein in *S. cerevisiae*. For this purpose, plasmids pAHG (*CYC1* promoter + *ubiG*), pQMG (*CYC1* promoter + *ubiG* with 5'-end sequence encoding the COQ3 N-terminal mitochondrial targeting signal), and pAH3

(*CYC1* promoter + *COQ3*), provided by Dr. Catherine Clarke (University of California, Los Angeles) (HSU *et al.* 1996), were used. The sequence encoding the AMC1 N-terminus (1-59 amino acids) was amplified, using the primers PHA-F and PHA-R, from a plasmid containing a cloned fragment of the *AMC1* cDNA (see Method S6). The PCR product was cloned into the *Hin*dIII site of the plasmid pAHG (HSU *et al.* 1996), carrying the *ubiG* gene under the control of the constitutive *CYC1* promoter, by In-Fusion Cloning (In-Fusion HD cloning kit, Clontech, 639648). The resulting construct, containing the sequence corresponding to 1-59 amino acids of AMC1 at the 5'-end of the *ubiG* gene, is referred to as pAHG59. The pAHG, pQMG, pAH3, and pAHG59 plasmids, each containing the *URA3* selectable marker, were introduced into the *Δcoq3* strain by one-step transformation (CHEN *et al.* 1992).

SUPPLEMENTAL INFORMATION REFERENCES

Allen, M. D., J. Kropat, S. Tottey, J. A. Del Campo and S. S. Merchant, 2007 Manganese deficiency in Chlamydomonas results in loss of photosystem II and MnSOD function, sensitivity to peroxides, and secondary phosphorus and iron deficiency. Plant Physiol 143**:** 263-277.

Altschul, S. F., W. Gish, W. Miller, E. W. Myers and D. J. Lipman, 1990 Basic local alignment search tool. J Mol Biol 215**:** 403-410.

Bailey, T. L., M. Boden, F. A. Buske, M. Frith, C. E. Grant *et al.*, 2009 MEME SUITE: tools for motif discovery and searching. Nucleic Acids Res 37**:** W202-208.

Blaby, I. K., C. E. Blaby-Haas, N. Tourasse, E. F. Hom, D. Lopez *et al.*, 2014 The Chlamydomonas genome project: a decade on. Trends Plant Sci 19**:** 672-680.

Boratyn, G. M., A. A. Schaffer, R. Agarwala, S. F. Altschul, D. J. Lipman *et al.*, 2012 Domain enhanced lookup time accelerated BLAST. Biol Direct 7**:** 12.

Chen, D. C., B. C. Yang and T. T. Kuo, 1992 One-step transformation of yeast in stationary phase. Curr Genet 21**:** 83-84.

Dent, R. M., C. M. Haglund, B. L. Chin, M. C. Kobayashi and K. K. Niyogi, 2005 Functional genomics of eukaryotic photosynthesis using insertional mutagenesis of *Chlamydomonas reinhardtii*. Plant Physiol 137**:** 545-556.

Gabilly, S. T., J. Kropat, M. Karamoko, M. D. Page, S. S. Nakamoto *et al.*, 2011 A novel component of the disulfide-reducing pathway required for cytochrome c assembly in plastids. Genetics 187**:** 793-802.

Harris, E. H., 1989 *The Chlamydomonas Sourcebook: A comprehensive guide to biology and laboratory use*. Academic Press, San Diego, CA.

Hsu, A. Y., W. W. Poon, J. A. Shepherd, D. C. Myles and C. F. Clarke, 1996 Complementation of coq3 mutant yeast by mitochondrial targeting of the Escherichia coli UbiG polypeptide: evidence that UbiG catalyzes both O-methylation steps in ubiquinone biosynthesis. Biochemistry 35**:** 9797-9806.

Liu, Y. G., N. Mitsukawa, T. Oosumi and R. F. Whittier, 1995 Efficient isolation and mapping of *Arabidopsis thaliana* T-DNA insert junctions by thermal asymmetric interlaced PCR. Plant J. 8**:** 457-463.

Livak, K. J., and T. D. Schmittgen, 2001 Analysis of relative gene expression data using real-time quantitative PCR and the 2(-Delta Delta C(T)) Method. Methods 25**:** 402-408.

Newman, S. M., J. E. Boynton, N. W. Gillham, B. L. Randolph-Anderson, A. M. Johnson *et al.*, 1990 Transformation of chloroplast ribosomal RNA genes in Chlamydomonas: molecular and genetic characterization of integration events. Genetics 126**:** 875-888.

Purton, S., and J. D. Rochaix, 1994 Complementation of a *Chlamydomonas reinhardtii* mutant using a genomic cosmid library. Plant Mol. Biol. 24**:** 533-537.

Sambrook, J., E. F. Fritsch and T. Maniatis, 1989 *Molecular Cloning A Laboratory Manual*. Cold Spring Harbor Laboratory Press, New York.

Schmollinger, S., T. Muhlhaus, N. R. Boyle, I. K. Blaby, D. Casero *et al.*, 2014 Nitrogen-Sparing Mechanisms in Chlamydomonas Affect the Transcriptome, the Proteome, and Photosynthetic Metabolism. Plant Cell 26**:** 1410-1435.

Valledor, L., T. Furuhashi, A. M. Hanak and W. Weckwerth, 2013 Systemic cold stress adaptation of Chlamydomonas reinhardtii. Mol Cell Proteomics 12**:** 2032-2047.

Werner, R., and D. Mergenhagen, 1998 Mating Type Determination of Chlamydomonas reinhardtii by PCR. Plant Molecular Biology Reporter 16**:** 295-299.

Wobbe, L., and P. J. Nixon, 2013 The mTERF protein MOC1 terminates mitochondrial DNA transcription in the unicellular green alga Chlamydomonas reinhardtii. Nucleic Acids Res 41**:** 6553-6567.